Research Square

Preprints are preliminary reports that have not undergone peer review.
They should not be considered conclusive, used to inform clinical practice,
or referenced by the media as validated information.

# Metabolic Reprogramming by Time-Restricted Fasting Attenuates Astrocytic Oxidative Stress and Mitochondrial Apoptosis after Ischemic Stroke via BDH1/SLFN2/NRF2 Axis

**Han Yin**

yinhan912@163.com

Harbin Medical University

**Yingying Zhang**

Harbin Medical University

**Hui Ci**

Harbin Medical University

**Kun Li**

Harbin Medical University

**Haiyu Zhang**

First Affiliated Hospital of Harbin Medical University

**Jinrong Wu**

First Affiliated Hospital of Harbin Medical University

**Xinmin Zhang**

Harbin Medical University

**Hang Yang**

Harbin Medical University

**Qian Yu**

Harbin Medical University

**Dandan Wang**

First Affiliated Hospital of Harbin Medical University

**Shanshan Yang**

First Affiliated Hospital of Harbin Medical University

**Guangyou Wang**

Harbin Medical University

**Tongshuai Zhang**

Harbin Medical University

**Research Article**

**Keywords:** Ischemia-Reperfusion Injury, Time-Restricted Fasting, Metabolic reprogramming, BDH1, Oxidative stress

**Posted Date:** October 19th, 2026

**DOI:** https://doi.org/10.21203/rs.3.rs-10716198/v1

**License:** This work is licensed under a Creative Commons Attribution 4.0 International License. Read Full License

**Additional Declarations:** No competing interests reported.

# Abstract

Metabolic disturbances in the brain and peripheral tissues after ischemic stroke exacerbate secondary brain injury and impede neurological recovery; however, effective targets and practical strategies for correcting these disturbances remain lacking. By integrating Bulk RNA sequencing, single-nucleus RNA sequencing (snRNA-seq), and Mendelian randomisation analysis, we found that glycolipid metabolism in the nervous system is severely disrupted after stroke, with substantial differences across cell types. We subsequently investigated whether Time-Restricted Fasting (TRF), a dietary regimen known to improve metabolic health, could restore metabolic homeostasis after stroke. TRF significantly alleviated post-stroke metabolic dysregulation and, unexpectedly, increased the production of endogenous ketone bodies and their utilisation in neural tissues. In this response, BDH1, a key enzyme involved in ketone-body utilisation in astrocytes, was linked to post-stroke metabolic imbalance and oxidative stress injury: silencing BDH1 in astrocytes markedly exacerbated post-stroke oxidative stress and mitochondria-dependent apoptosis. We also observed that semaglutide prevented cerebral ischemia-reperfusion injury, an effect that may be attributable to its improvement of glucose homeostasis and enhancement of ketone metabolism.


# Introduction

Acute ischemic stroke (AIS) remains a life-threatening cerebrovascular disease. When cerebral blood vessels become occluded, local ischemia and hypoxia ensue, constituting the core events that trigger neuronal injury. As oxygen and glucose can no longer be effectively utilised, mitochondrial aerobic respiration fails, and adenosine triphosphate (ATP) is rapidly depleted; anaerobic glycolysis increases as a compensatory response but leads to the accumulation of large amounts of lactate and reactive oxygen species [1, 2]. Meanwhile, ischemia drives abnormally increased fatty acid oxidation. At the same time, excessive lipid peroxides and reactive oxygen species generated through peroxidation further exacerbate oxidative stress and mitochondrial dysfunction, ultimately leading to neuronal death. This dual dysregulation of glucose and lipid metabolism is a key driver of post-stroke neuronal injury and worsens patient outcomes [3–5]. Mechanical thrombectomy and intra-arterial thrombolysis remain the main treatments for AIS; however, the narrow therapeutic window and severe postoperative complications mean that fewer than half of patients can benefit from these interventions. Therefore, improving stroke outcomes remains an urgent clinical challenge, underscoring the pressing need for new strategies to restore metabolic homeostasis.

Time-restricted feeding (TRF) is a dietary intervention that rhythmically regulates systemic metabolic homeostasis by controlling the timing of food intake. Once the fasting period exceeds 12 hours, hepatic glycogen stores become completely depleted, forcing the body to shift from reliance on glucose to fatty acid oxidation and ketone body production[6]. This metabolic switch between glucose and lipid utilisation not only provides an alternative fuel source but is also accompanied by regulatory adjustments in cellular adaptive stress pathways. It has been reported that time-restricted feeding can improve systemic insulin sensitivity, promote fat oxidation, and activate autophagy pathways by

reshaping metabolic rhythms, thereby optimising energy metabolism at the systemic level[7, 8]. In the brain, time-restricted feeding can alleviate lipopolysaccharide-induced oxidative stress and upregulate neurotrophic factors (BDNF and FGF2) and antioxidant enzymes (HO-1), thereby exerting protective effects against various neurological disorders[9–11]. However, the neuroprotective effects of time-restricted feeding in ischemic stroke remain unclear.

Astrocytes are the most abundant glial cells in the brain and possess a powerful capacity to regulate fatty acid metabolism. They are considered the primary cells responsible for ketone body synthesis and utilisation in the brain [12]. Following TRF-mediated glucose–lipid switching, ketone bodies become an important fuel for the brain and are essential for maintaining neuronal function [13, 14]. BDH1 (β-hydroxybutyrate dehydrogenase 1) catalyses the interconversion of ketone bodies in mammals. It is highly expressed in the mitochondrial matrix of the liver, heart, skeletal muscle, and brain, where it plays a central role in fatty acid oxidation and ketone body metabolism [15, 16]. Studies of breast cancer and melanoma have shown that dietary restriction can increase β-hydroxybutyrate levels among ketone bodies, thereby enhancing antitumor immune responses, because BDH1-mediated ketolysis can reprogram CD8 + T-cell metabolism and promote mitochondrial oxidative phosphorylation and effector functions [17, 18]. BDH1 activity also depends strongly on the mitochondrial NAD+/NADH ratio, placing BDH1 at the intersection of energy metabolism and redox homeostasis [19]. In models of diabetic kidney disease and heart failure, BDH1-mediated ketone body metabolism has been shown to alleviate oxidative stress, inflammation, and apoptosis by activating the NRF2 pathway [20]; in models of ischemic stroke, exogenous βOHB administration can reduce infarct volume and improve neurological function. However, whether BDH1 in astrocytes is a key target of TRF-mediated neuroprotection remains unclear.

This study aimed to investigate the role of BDH1 as a regulatory target of TRF in ischemic stroke. By selectively modulating BDH1 expression in astrocytes, we found that BDH1 serves as a central hub through which TRF suppresses oxidative stress and mitochondrial apoptosis following ischemia/reperfusion. We further identified a cytoplasmic protein, Schlafen 2 (SLFN2), as a key downstream signalling effector of BDH1 in the oxidative stress response. These findings reveal a previously unrecognised mechanism whereby TRF exerts neuroprotective effects by activating the BDH1/ketone body metabolism pathway in astrocytes, and provide a noninvasive, highly compliant therapeutic strategy for acute ischemic stroke (AIS).

# Methods

## 1. Animals

Male C57BL/6JWT mice aged 8 to 10 weeks were obtained from Liaoning Changsheng Company (Liaoning, China) and housed in an SPF-grade animal facility at 22–24°C with 50–60% relative humidity under a 12-hour light-dark cycle, with free access to food and water. Adeno-associated virus (AAV9-GFP-shBdh1) and the corresponding control virus (AAV9-GFP-shNC) were purchased from Vigen

Biotechnology (Jinan, China). Three weeks before eTRF, 1.5 μL of virus was stereotactically injected into the lateral ventricle of C57BL/6JWT mice (coordinates: X = 1.5 mm, Y=-1.1 mm, Z=-2.0 mm). The Ethics Committee of Harbin Medical University approved all animal experiments.

## 2. Time Restricted Fasting Treatment

Male mice weighing 15–17 g were randomly allocated to two groups: ad libitum (A/L) feeding and early Time-Restricted Fasting (eTRF, ZT10-ZT18). eTRF was scheduled according to the circadian rhythm of the mice; the animals could obtain food only within the designated window, with no restriction on food amount, and water was available at all times. After this regimen had been maintained for 4 weeks, the mice were allowed to feed adequately for two hours, and a cerebral I/R injury model was then established using the filament occlusion method. Food access was no longer restricted after modeling, and samples were collected at the indicated time points.

## 3. Establishment of the I/R Injury Model by Filament Occlusion

Mice were anesthetized with 4% tribromoethanol (1.5 ml/kg). A midline neck incision was made under a stereomicroscope to expose and ligate the common carotid artery, internal carotid artery, and external carotid artery. An embolus was advanced into the internal carotid artery to occlude the middle cerebral artery (MCA). The filament was withdrawn after one hour of occlusion to allow reperfusion of the common carotid artery, and all incisions were then sutured[21].

## 4. Behavioral Experiments

The mNSS scoring, cylinder test, and open field test were performed 24 hours after the mouse cerebral I/R model was established. The mNSS is a widely used tool for grading neurological deficits in experimental animals and mainly covers motor function, sensory function, and reflexes. The detailed procedures were as follows:

Motor function assessment: the mouse was placed on the floor. Normal walking was scored 0; inability to walk in a straight line, 1; circling toward the paralyzed side, 2; and falling toward the paralyzed side, 3.

Tail suspension test: abnormal flexion or rigidity of the forelimbs or hindlimbs was scored 1 point, and deviation of the head from the vertical axis by more than 10 degrees was scored 1 additional point.

Balance beam test: the posture of the mouse on the balance beam was observed. A stable posture with straight walking was scored 0; gripping the edges of the beam, limbs slipping off, nearly falling, and actual falling were scored 1 to 6 points, respectively.

Reflex function test: the auricular reflex (avoidance behavior when the outer ear canal is touched) and the corneal reflex (blinking when the cornea is touched) were examined; a present reflex was scored 0

and an absent reflex 1 point.

## Cylinder test:

Each mouse was placed in a transparent resin glass cylinder for 3–10 minutes and recorded on video, and the number of times the mouse touched the cylinder wall with its forelimbs within three minutes after rearing was documented. Contacts made by the left, right, and affected forelimbs were counted separately, and the percentage of sole ipsilateral forelimb wall contacts was compared with that of sole contralateral contacts to obtain the asymmetry index.

## Field experiment

Each mouse was placed in the center of the open field apparatus, and its behavior was recorded with a camera for 5 minutes. The measurements included the total distance traveled, average speed, and the time spent in the center and at the edges of the field. Movement trajectories and dwelling areas were then analyzed from the video footage together with the data from motion tracking software.

# 5. TTC (Triphenyl Tetrazolium Chloride)

Mice were euthanized by cervical dislocation, and the brain was rapidly removed after decapitation and placed in a pre-cooled stereotaxic mold (RWD, China). Continuous coronal sections of fixed thickness were cut starting from the origin of the olfactory bulb. The sliced brain sections were immediately immersed in 2% TTC staining solution (Sigma-Aldrich, USA) along the same direction; once the color contrast was most prominent, the dye solution was discarded and the slices were fixed with 4% paraformaldehyde. The infarct area was calculated with ImageJ.

# 6. Primary Cell Isolation and Culture

Primary astrocytes were isolated from newborn C57BL/6 pups younger than three days. The cerebral cortex was dissected aseptically after surface sterilization with 75% ethanol and transferred into F12 culture medium. The tissue was mechanically dissociated into a single-cell suspension, filtered through a 40-micron cell strainer, and centrifuged at 1600 rpm for 5 minutes; the resulting pellet was resuspended and seeded into poly-D-lysine-coated culture flasks. Following overnight incubation and 7–8 days of further culture, the cells were passaged and purified until confluent and then randomly assigned to control and experimental groups. The low-glucose group received a serum-free medium in which glucose-free culture solution and F12 were mixed at a 10:1 ratio to yield a final glucose concentration of 1.75 mM; after penicillin-streptomycin supplementation, the cells were cultured for 12 hours to mimic in vivo fasting conditions.

# 7. Oxygen-Glucose Deprivation (OGD) Experiment

To simulate ischemic conditions in vitro, oxygen-glucose deprivation (OGD) experiments were conducted. The original culture medium was replaced with glucose-free medium, and the cells were incubated at 37°C in a hypoxic chamber containing 95% nitrogen (N2) and 5% carbon dioxide (CO2).

# 8. Plasmid Transfection

SiRNAs targeting Bdh1, Slfn2, and the negative control (NC) (GenePharma, China) were transfected into cells with Lipofectamine 3000 (Invitrogen, USA).

## siRNA sequence

mouse-Bdh1 sense(5'-3'): GCCAUCGCCAAGAAGAUGUTT

mouse-Bdh1 antisense(5'-3'): ACAUCUUCUUGGCGAUGGCTT

mouse-Slfn2 sense(5'-3'): CCCUUUACCAGAUCCAGAUTT.

mouse-Slfn2 antisense(5'-3'): AUCUGGAUCUGGUAAAGGGTT

# 9. Cell Viability Assay

Primary astrocytes were seeded into 96-well plates and allowed to adhere fully, after which 10 μL of Cell Counting Kit-8 (CCK-8, TargetMol, USA) reagent was added to each well. Following incubation at 37°C for 2 hours, the absorbance at 450 nm was measured on a microplate reader, and cell viability was expressed as a percentage relative to the control wells.

# 10. Quantitative real-time PCR

Total RNA was extracted from cells and tissues with Trizol reagent (Invitrogen, 15596026). RNA concentration and purity were determined on a Nano-300 instrument (Everest, China), and RNA integrity was checked by agarose gel electrophoresis. cDNA was synthesized from 2 μg of RNA using the Revertaid First Strand cDNA Synthesis Kit (Thermo, USA), and gene expression was quantified by qPCR with ChamQ SYBR qPCR Master Mix (Vazyme, China). The qPCR primers used here are provided in Supplementary Table 1.

# 11. Western blot

Mitochondrial and nuclear proteins were extracted according to the kit instructions (Beyotime, China). The supernatant was mixed with loading buffer and boiled at 95°C for 15 minutes, and the protein

concentration was determined with the BCA Protein Assay Kit (Beyotime, China) by measuring absorbance at 562 nm. The protein samples were separated by 10% sodium dodecyl sulfate-polyacrylamide gel electrophoresis (SDS-PAGE) and transferred onto polyvinylidene fluoride (PVDF) membranes. The membranes were blocked with 5% skim milk powder for 30 minutes at room temperature, incubated overnight at 4°C with the primary antibody, and then incubated with the corresponding secondary antibody. Protein signals were detected on a ChemiScope 6000 series instrument (Clinx, China), and protein levels were quantified with the ChemiScope image analysis software. All antibodies used in this study are listed in Supplementary Table 2.

## 12. Immunofluorescent staining

Mouse brain tissue was rapidly frozen in liquid nitrogen, and 10 μm frozen sections were prepared on a cryostat. Cells were cultured on glass-bottom dishes or coverslips. Fixation was performed with 4% paraformaldehyde for 5 minutes, and blocking and staining were carried out at room temperature with 0.5% Triton X-100 and 5% BSA. Primary antibody, secondary antibody, and DAPI staining were performed according to the target protein. The CM-H2DCF-DA probe and JC-1 probe (Beyotime, China) were incubated at 37°C for 30 minutes to assess intracellular ROS levels and changes in mitochondrial membrane potential, and apoptosis in tissue was analyzed with a fluorescent TUNEL assay kit (Beyotime, China). Images were acquired with an Olympus FV3000 laser scanning confocal microscope and processed using FV31S-SW software. The antibodies used here are provided in Supplementary Table 2.

## 13. Metabolomics

Metabolomic analysis was conducted by Shanghai Baiqu Biotechnology Co., Ltd. Briefly, cortical tissue samples from the cerebral infarction area of mice in the ad libitum feeding and TRF groups were collected. A 25 mg portion of each sample was accurately weighed into an EP tube at low temperature, two homogenizing beads were added, followed by 500 μL of extraction solvent (methanol:acetonitrile:water = 2:2:1 [v/v]) containing isotope-labeled internal standards. The samples were vortexed for 30 seconds, homogenized in a tissue grinder (35 Hz, 4 minutes), and sonicated in an ice-water bath for 5 minutes; this step was repeated three times. After incubation at -40°C for one hour, the samples were centrifuged at 4°C for 15 minutes at 12,000 rpm (~ 13,800 × g; rotor radius 8.6 cm), and the supernatant was transferred to vials for analysis on a Vanquish Ultra-High Performance Liquid Chromatography system (Thermo Fisher Scientific, USA). Equal volumes from all supernatants were pooled as QC samples and analyzed under the same conditions. The raw data were converted to mzXML format with ProteoWizard software, metabolites were identified using a collaboratively developed R package together with the BiotreeDB (V3.0) database, and visualization was performed with a self-developed R package.

## 14. Transcriptomics

Transcriptomic sequencing was conducted by Shanghai Baiqu Biotechnology Co., Ltd. In brief, total RNA was extracted with Trizol (Thermo Fisher Scientific, USA) from astrocytes after OGD and from siBdh1 + OGD astrocytes. RNA quantity and purity were assessed on a NanoDrop ND-1000 (NanoDrop, Wilmington, DE, USA), and RNA integrity was evaluated with a Bioanalyzer 2100 (Agilent, CA, USA). Paired-end sequencing was carried out on the Illumina Novaseq™ 6000 in PE150 mode following standard protocols. The sequencing data were filtered to retain high-quality reads, which were then aligned to the reference genome of the species used in this project; gene expression quantification, differential gene analysis, enrichment analysis, and related analyses were subsequently performed.

## 15. Data Analysis

All experiments were independently repeated at least three times. Statistical analyses were performed with GraphPad Prism 9.0 software, and the data are presented as mean ± standard deviation. The Shapiro-Wilk test was used to assess the normality of data distributions. For comparisons among multiple groups, one-way analysis of variance (ANOVA) was performed, followed by Tukey's multiple comparison test to determine significant differences between groups. When the data did not meet the assumption of normality, non-parametric tests (such as the Kruskal-Wallis test) were applied, followed by Dunn's post hoc test. A p-value below 0.05 was considered statistically significant, and significance levels are denoted by $^{*}P < 0.05$, $^{**}P < 0.01$, and $^{***}P < 0.001$, respectively.

## Result

1. **Bulk Transcriptomics Combined with Mendelian Randomization Reveals the Metabolic Signature of Cerebral Ischemia**

To characterize how metabolic pathways change over time after cerebral ischemia, we examined three core metabolic pathways, namely glycolysis, oxidative phosphorylation, and fatty acid metabolism, using bulk transcriptomic sequencing data (GSE233811). Principal component analysis separated the samples clearly by time point (Figure s1A). Using gene sets extracted from the MSigDB database, we mapped the expression changes at five post-stroke time points (3 h, 12 h, 24 h, 3 d, and 7 d) with heatmaps and line plots (Fig. 1A–C). Glycolysis began to rise at 24 h and peaked at 3 d; oxidative phosphorylation fell significantly at 12 h and then recovered at 24 h; fatty acid metabolism tracked oxidative phosphorylation closely, decreasing at 12 h before climbing continuously from 24 h to 7 d. GSEA at the key time points corroborated these patterns: glycolysis was significantly enriched at 24 h and 3 d, oxidative phosphorylation showed negative enrichment at 12 h with recovery after 24 h, and fatty acid metabolism became significantly enriched from 24 h onward (Figure s1B–E). Together, these data indicate a temporal metabolic reprogramming after stroke.

To relate these metabolic changes to post-stroke pathological processes, we computed Pearson correlations between each metabolic pathway and the inflammation, apoptosis, and reactive oxygen species (ROS) pathways (Fig. 1D–F). Glycolysis showed a significant positive correlation with all three pathological pathways, most strongly with inflammation. Fatty acid metabolism likewise showed significant positive correlations, with the most pronounced effect on ROS. In contrast, higher oxidative phosphorylation was significantly associated with lower apoptosis. These observations suggest that post-stroke metabolic reprogramming, particularly the upregulation of glycolysis and fatty acid metabolism, may aggravate tissue injury by fueling inflammation and oxidative stress.

In contrast, restoration of oxidative phosphorylation may be protective. To test whether glycolipid metabolism disorders exert independent causal effects on cerebral ischemia, we performed two-sample Mendelian randomisation (MR) analyses, using diabetes (approximately 38 SNPs) and hyperlipidemia/lipoprotein metabolism disorders (20 SNPs) as exposures and cerebral ischemia as the outcome. In leave-one-out sensitivity analysis, the pooled effect estimates under both exposures remained stable when any single SNP was removed, with all estimates pointing in the same direction; in the lipoprotein metabolism disorder analysis, every P-value was < 0.05, indicating high robustness that was not driven by any individual SNP (Figure s2A, Figure s2E). In the forest plots, the MR-Egger pooled point estimates were all positive. However, they had confidence intervals containing 1 (lipoprotein metabolism disorder: OR = 1.15, 95% CI: 0.99–1.33, $P$ = 0.093), whereas the IVW pooled point estimates were positive (approximately + 0.10 for diabetes and 0.115 for hyperlipidemia/lipoprotein metabolism disorder; OR = 1.12), with confidence intervals excluding 1 and reaching statistical significance ($P$ = 0.001), consistent with a positive causal association of both exposures with stroke risk (Figure s2B, Figure s2F). Funnel plots were approximately symmetric around the reference line;. However, the lipoprotein metabolism disorder analysis showed some heterogeneity (Cochran's Q test $P$ < 0.001), there was no indication of systematic bias or publication bias (Figure s2C, Figure s2G). In the scatter plots, the IVW and MR-Egger regression lines had positive slopes in highly consistent directions, and the MR-Egger intercepts in the diabetes and lipoprotein metabolism disorder analyses were close to zero, arguing against horizontal pleiotropy and further supporting the robustness of the causal effects (Figure s2D, Figure s2H). Overall, the IVW results support that both glycolipid metabolism disorders are risk factors for cerebral ischemia..

## 2. Single-Nucleus Transcriptomics Reveals Cell Type–Specific Metabolic Reprogramming After Cerebral Ischemia

To resolve the metabolic dynamics after cerebral ischemia at single-cell resolution, we performed a secondary analysis of single-nucleus RNA sequencing data from the public dataset GSE279666. After quality control, principal component analysis (PCA) of highly variable genes clearly separated the samples along PC1, with CI_Day3 and CI_Day14 forming distinct clusters, indicating temporal transcriptomic dynamics after ischemic injury (Figure s2I). UMAP dimensionality reduction and visualisation identified seven major cell types; excitatory neurons accounted for the largest proportion,

followed by astrocytes, inhibitory neurons, and microglia (Figure s2J). The expression of canonical marker genes in each cell type confirmed the accuracy of the annotation (Figure s2K).

To gauge global metabolic activity, 1,595 metabolism-related genes were extracted from the MSigDB database; their mean expression per cell served as a metabolic activity score, which was projected onto the UMAP space (Fig. 2A). The distribution of metabolic activity across the entire cell population was highly heterogeneous: high-activity cells clustered mainly in regions enriched for astrocytes and microglia, whereas low-activity cells were scattered across neuron-rich areas. Screening each cell type for differentially expressed metabolic genes revealed a unique metabolic gene expression profile for every cell type (Fig. 2B). Integration of 28 MSigDB metabolic pathways in a horizontal dot plot (Fig. 2C) showed significant activation of core energy metabolism pathways, including glycolysis, oxidative phosphorylation, and lipid metabolism, in astrocytes. In contrast, microglia were enriched for amino acid and nucleotide metabolism, suggesting a functional division of metabolic labour among the major cell types in brain tissue.

We next focused on astrocytes and microglia, the cell types that responded most strongly after ischemia. We used the AUCell algorithm to track their pathway activity scores from the healthy and sham conditions through the acute and recovery phases. In astrocytes, glycolysis was mildly upregulated during the acute phase relative to controls and then fell by nearly 50% during the recovery phase; TCA cycle activity declined continuously; and fatty acid β-oxidation activity decreased gradually, ending approximately 25% below control levels after ischemia (Fig. 2D). These data indicate that astrocytes undergo metabolic reprogramming after cerebral ischemia, with compensatory enhancement of glycolysis in the acute phase, sustained suppression of aerobic metabolism, and a return of glycolysis toward baseline during recovery. However, overall energy metabolism remained lower than normal. Microglia behaved differently, displaying a characteristic immune-metabolic activation profile in which glycolysis and fatty acid oxidation were significantly enhanced during the acute phase while TCA cycle activity remained relatively stable; this pattern reflects a metabolic shift toward a pro-inflammatory phenotype that supports inflammatory responses and phagocytic function. Such cell–type–specific metabolic dynamics provide a basis for targeted metabolic interventions (Fig. 2E).

## 3. Time-Restricted Fasting Attenuates Cerebral Ischemia-Reperfusion Injury and Restores Neural Metabolic Homeostasis

C57BL/6 mice were first randomly assigned to an ad libitum (A/L) feeding group or an early Time-Restricted Fasting (eTRF) group. eTRF mice could obtain food only between ZT10 and ZT18, whereas the A/L group faced no feeding time restriction; all animals had free access to water. After four weeks of intervention, a cerebral ischemia (1 h)-reperfusion (2 d) injury (I/R) model was established, and on the day before modelling, all groups were allowed unrestricted food intake. The experimental design is illustrated in Fig. 3A. To determine whether TRF mice differed from A/L mice in total food intake or feeding rhythm, we monitored food consumption and feeding time over 24 hours. Although eTRF mice

could eat for only eight hours per day, total food consumption did not differ significantly between the two groups (Figure s3A). Feeding rhythm, assessed by hourly weighing of the remaining food, showed that eTRF mice ate mainly at one hour and six hours after food access was resumed, whereas A/L mice exhibited no distinct feeding peaks (Fig. 3B). Body weight was monitored after two and four weeks of fasting intervention and decreased significantly in the eTRF group at both time points (Fig. 3C).

To test whether Time-Restricted Fasting ameliorates cerebral I/R injury, we established an I/R (2 d) model in each group. We comprehensively evaluated functional recovery using TTC staining, the modified Neurological Severity Score (mNSS), the cylinder test, and the open field test. TTC staining showed a significantly smaller cerebral infarct volume in the eTRF group than in the A/L group (Fig. 3D). The cylinder test and mNSS scores indicated that motor function, sensory function, and reflexes were significantly better in eTRF mice than in A/L mice (Fig. 3E–F). The open field test supported the same conclusion: compared with the A/L group, eTRF mice showed significantly greater total movement time and average speed, together with significantly reduced resting time (Fig. 3G–J). These results indicate that early Time-Restricted Fasting outperforms ad libitum feeding in ameliorating I/R injury.

After I/R injury, transient blood reperfusion severely disrupts glycolipid metabolic homeostasis in the core lesion and penumbra, provoking oxidative stress and neuroinflammation that further aggravate brain injury[1]. We therefore examined how Time-Restricted Fasting affects glycolipid metabolism after I/R. Serum biochemical assays in sham and I/R (2 d) mice (Fig. 3K–M) showed significantly lower blood glucose in the eTRF group than in the A/L group. In the non-ischemic state, eTRF decreased free fatty acid levels; after I/R injury, eTRF significantly normalised free fatty acids, while triglycerides remained comparable between the A/L and eTRF groups. These findings suggest that Time-Restricted Fasting markedly regulates glycolipid metabolic homeostasis after I/R injury. Having confirmed the metabolic regulatory effects of fasting in the peripheral circulation, we next turned to the central nervous system. Carnitine palmitoyltransferase (CPT), peroxisome proliferator-activated receptor-γ coactivator-1α (Pgc-1α), and glucose transporter (Glut) mediate the transmembrane transport of fatty acids and glucose. Under physiological conditions, qPCR analysis (Figure s3B) showed that, relative to the A/L group, the eTRF group had significantly upregulated Cpt1, Cpt2, and Pgc-1α and significantly downregulated Glut3, with Glut1 unchanged. We next established the I/R model in each group to evaluate how fasting shapes neural glycolipid metabolism after I/R. The qPCR results under pathological conditions were strikingly different: Cpt1 and Cpt2 expression levels in the eTRF group were significantly lower than those in the A/L group, whereas Glut3 expression was significantly upregulated (Fig. 3N). In light of changes in free fatty acids and glucose detected in serum biochemical assays, we hypothesise that alterations in Cpt1, Cpt2, and Glut3 after I/R represent compensatory adjustments to altered substrate availability, helping cells adapt their energy substrate supply. Taken together, these results indicate that Time-Restricted Fasting downregulates glucose metabolism in the nervous system and ameliorates post-I/R lipid metabolism disturbances.

To further validate these findings, untargeted metabolomic profiling was performed on the ipsilateral cerebral cortex of A/L and eTRF mice after I/R injury. Principal component analysis (PCA) clearly

separated the two groups, with tight intragroup clustering (Figure s3C), indicating that the eTRF intervention substantially remodelled the brain metabolomic profile of I/R mice. Volcano plot analysis identified 125 differential metabolites (Fig. 3O). With respect to glucose metabolism, eTRF reduced several phosphorylated monosaccharides, curbed aberrant glycolysis and the pentose phosphate pathway, and significantly enriched fructose and mannose metabolism, as well as glycolysis/gluconeogenesis, thereby alleviating glucose metabolic disturbances. With respect to lipid metabolism, acyl-carnitines, the intermediates of fatty acid β-oxidation that accumulate when mitochondrial fatty acid oxidation is impaired, were downregulated by eTRF, suggesting improved mitochondrial function and more complete fatty acid oxidation after I/R injury. eTRF also raised specific hydroxy fatty acids, including 2-hydroxypalmitic acid and 16-hydroxypalmitic acid, which may act as alternative energy substrates that support ischemic brain tissue while reducing reactive oxygen species (ROS) production, thereby exerting neuroprotective effects (Fig. 3P, Figure s3D-H). Pathway enrichment analysis showed significant modulation of lipid metabolism pathways, including arachidonic acid metabolism and glycerophospholipid metabolism. For bile acids, eTRF downregulated glycolithocholic acid 3-sulfate and tauroursodeoxycholic acid, which may contribute to neuroprotection through the gut-brain axis. Collectively, these results demonstrate that eTRF ameliorates glycolipid metabolic disturbances in a multidimensional manner (Fig. 3Q).

## 4. Astrocytic BDH1 Mediates the Ameliorating Effect of Time-Restricted Fasting on Cerebral Ischemia-Reperfusion Injury

During cerebral ischemia, vascular occlusion deprives the corresponding region of the blood supply of oxygen and glucose. Mechanical reperfusion can partially restore blood flow, but the ischemic core and penumbra remain in a low-oxygen, low-glucose state due to tissue no-reflow and other factors, leading to energy depletion [22]. We therefore asked whether Time-Restricted Fasting could improve energy supply in the injured region. Lactate, a key product of anaerobic oxidation, was measured first. As shown in Figure s3I, Time-Restricted Fasting did not affect lactate accumulation under physiological conditions; in the I/R group, lactate rose significantly, and eTRF intervention significantly reversed this increase. We next measured acetyl-CoA, a key substrate of aerobic oxidation, together with ATP production. Aerobic energy production centres on the tricarboxylic acid (TCA) cycle and oxidative phosphorylation; because acetyl-CoA initiates the TCA cycle, it critically determines aerobic oxidation and energy supply. Acetyl-CoA synthetase activity was therefore measured to determine the effect of eTRF on acetyl-CoA expression. The activity was comparable between the eTRF and A/L groups under physiological conditions (Fig. 4A) but rose significantly in the eTRF group after I/R injury. ATP production, however, remained comparable between the two groups after I/R injury (Fig. 4B). Metabolomic data further showed that eTRF significantly lowered the TCA cycle intermediates citrate and isocitrate in the mouse cerebral cortex, even though pathway analysis detected no significant change in the TCA cycle itself (Figure s3J-K). Thus, despite increasing acetyl-CoA expression, eTRF does not elevate ATP levels after I/R injury, most likely because the TCA cycle is not effectively activated (Figure s3L). Having found that eTRF does not alter ATP production after I/R injury, we next explored whether the elevated acetyl-CoA

might be directed toward other pathways. Ketone bodies are downstream products of lipid metabolism, largely derived from the oxidative breakdown of fatty acids, and acetyl-CoA also serves as a key substrate for their synthesis and utilisation [23]. Serum β-hydroxybutyrate was therefore measured: as expected, it was comparable between the eTRF and A/L groups under physiological conditions but rose significantly in the eTRF group after I/R injury (Fig. 4C). qPCR was then used to assess expression of cortical ketogenesis and ketolysis genes, including acetyl-CoA acetyltransferase 1 (ACAT1), succinyl-CoA transferase (SCOT), and β-hydroxybutyrate dehydrogenase 1 (BDH1). Acat1 and Scot were comparable between the A/L and eTRF groups under physiological conditions (Figure s4A), whereas after I/R injury eTRF transcriptionally activated both ACAT1 and SCOT. Notably, BDH1 was significantly upregulated by eTRF under both physiological and post-I/R conditions (Fig. 4D). These findings suggest an important role of Time-Restricted Fasting in promoting ketone body utilization in the nervous system. We next tracked BDH1 expression after I/R injury in mouse models at 1 d, 2 d, 4 d, and 7 d post-I/R by western blot. BDH1 was lowest on days 1 and 2 post-I/R and gradually returned to normal levels by days 3–7 (Figure s4B), indicating marked suppression of BDH1 during the acute phase of stroke injury. At 2 days post-I/R, BDH1 protein was significantly higher in the eTRF group than in the A/L group (Fig. 4E). In addition to the liver's robust ketogenic capacity, astrocytes possess a complete fatty acid oxidation system and are regarded as key cells for cerebral ketone body breakdown and energy supply [13, 24]. We therefore explored whether eTRF enhances astrocytic BDH1. Immunofluorescence analysis showed significantly stronger BDH1 fluorescence colocalized with GFAP in the I/R+eTRF group than in the I/R + A/L group (Fig. 4F). Together, these results demonstrate that BDH1 expression falls and then recovers after I/R injury, and that eTRF intervention reverses this decline at its nadir (I/R 2 d).

Through the experiments described above, we comprehensively delineate how the glycolipid metabolic shift triggered by Time-Restricted Fasting leads to neural metabolic reprogramming after I/R injury. In brief, eTRF ameliorates post-stroke disturbances in glucose and fatty acid metabolism and promotes the activation of ketone metabolism, thereby achieving a switch in substrate utilization and neural metabolic reprogramming.

Having established the critical metabolic regulatory role of astrocytic BDH1 in eTRF, we next asked whether astrocytic BDH1 is the key target underlying the neuroprotective effect of Time-Restricted Fasting after I/R injury. We constructed an AAV9-GFabc9d-shBdh1-GFP adeno-associated virus and injected it stereotaxically into the lateral ventricle on the ischemic side to knock down BDH1 expression specifically in astrocytes. Three weeks after AAV injection, the mice underwent four weeks of eTRF intervention; the experimental timeline appears in Fig. 4G. Three weeks after AAV injection, we examined frozen sections for colocalization of intrinsic GFP fluorescence with GFAP, which verified the cell-type specificity of the knockdown (Fig. 4H-I): nearly all GFP signal overlapped with GFAP. We also examined GFP colocalization with BDH1 to assess whether the AAV successfully suppressed BDH1 expression. In the AAV-BDH1 group, the BDH1 signal colocalized with GFP was markedly suppressed, whereas the AAV-NC group showed clear colocalization of GFP with BDH1. These results confirm successful AAV-mediated knockdown of BDH1 in astrocytes. TTC staining was then used to determine changes in cerebral infarct volume after astrocytic BDH1 knockdown. As shown in Fig. 4J-K, Time-Restricted Fasting

significantly reduced cerebral infarct volume compared with the I/R group, whereas knockdown of astrocytic BDH1 significantly increased infarct volume. Motor function was subsequently assessed with the open field test. Under physiological conditions, motor activity did not differ significantly between the A/L and eTRF groups (Fig. 4L-M), but mice with astrocytic BDH1 knockdown showed a significant reduction in movement distance. After I/R injury, the eTRF group showed significant improvements in movement distance, average speed, and resting time, all of which were significantly reversed by astrocytic BDH1 knockdown. TUNEL staining supported the same conclusion: TUNEL-positive cells were significantly fewer in the eTRF group than in the I/R group and were significantly increased after astrocytic BDH1 knockdown (Fig. 4N-O). Neurological function was further assessed with the mNSS, and forelimb motor asymmetry with the cylinder test. As shown in Fig. 4P-Q, the eTRF group showed significantly improved mNSS scores relative to the I/R group.

In contrast, astrocytic BDH1 knockdown restored scores to levels comparable to those of the I/R group. The cylinder test confirmed that forelimb wall contacts on both sides improved significantly in eTRF mice compared with I/R mice, an effect not observed after astrocytic BDH1 knockdown. Collectively, these results demonstrate that AAV-mediated knockdown of astrocytic BDH1 partially abolishes the neuroprotective effects of Time-Restricted Fasting.

## 5. Transcriptomic Analysis Identifies Astrocytic BDH1 as a Key Regulator of Redox Homeostasis and Mitochondrial Function

After defining the principal biological functions of BDH1, we sought to reproduce the metabolic state induced by Time-Restricted Fasting in vitro. The results described above indicated that lowering blood glucose levels is a key initiating factor that triggers the glycolipid metabolic switch. According to the literature, culturing cells at glucose concentrations below 5 mM triggers a metabolic shift from glucose to glutamine metabolism[25]. We therefore investigated whether low-glucose stimulation could recapitulate the glycolipid metabolic switch induced by Time-Restricted Fasting. We first established serum-free, low-glucose culture conditions at glucose concentrations of 5.25, 3.5, and 1.75 mM and assessed astrocyte viability by CCK-8 assay at 12 h, 24 h, and 48 h to identify suitable conditions. As shown in Figure s4C, none of the three concentrations affected cell viability after 12 h of low-glucose culture. At 1.75 mM glucose, viability remained intact at 12 h but was significantly reduced at 24 h and declined further by 48 h. We therefore selected 1.75 mM glucose for 12 h as the low-glucose (LG) stimulation condition for subsequent experiments.

To determine whether a low-glucose state reproduces glycolipid metabolic changes in astrocytes, we compared glycolipid transport-related genes between the control (Ctrl) and LG groups by qPCR. Whether or not oxygen-glucose deprivation (OGD) was applied, LG stimulation significantly upregulated the fatty acid transport-related genes CPT1, CPT2, and PGC-1α and significantly downregulated the glucose transporter gene GLUT3 (Fig. 5A, Figure s4D). Ketone body-related genes behaved consistently with the in vivo results: their expression rose significantly after LG stimulation, and BDH1 showed the greatest

change (Fig. 5B, Figure s4E). Thus, culturing cells in low-glucose, serum-free medium successfully mimicked the post-fasting metabolic switch observed after in vivo Time-Restricted Fasting, and qPCR confirmed significant changes in glycolipid- and ketone body metabolism-related genes. We next asked whether LG stimulation alters astrocytic BDH1 expression. BDH1 rose progressively as the glucose concentration fell, and the fluorescence intensity of BDH1 colocalised with GFAP increased accordingly (Figure s4F-G). In astrocytes subjected to OGD for different durations, BDH1 increased gradually and peaked at 4 h, a pattern contrasting with the in vivo findings (Figure s5A). Extending this analysis to other resident brain cell types showed that microglia and neurons responded to OGD with BDH1 changes similar to those of astrocytes. In contrast, endothelial BDH1 decreased significantly after OGD (Figure s5B-D), implying that BDH1 may exert complex cell type-specific functions after stroke. Under OGD conditions, LG stimulation again upregulated BDH1 in a concentration-dependent manner, peaking at 1.75 mM (Fig. 5C), and immunofluorescence confirmed that BDH1 colocalised significantly with astrocytes (Fig. 5D). LG stimulation, therefore, significantly upregulates astrocytic BDH1 expression regardless of OGD injury. To test whether LG protects astrocytes, Ctrl and LG-pretreated cells underwent OGD for 4 h, and Bax, Bcl2, and caspase-3 were examined by western blot. OGD injury significantly upregulated caspase-3 and Bax, and these changes were significantly restored in the OGD + LG group (Figure s6A), indicating that the low-glucose state ameliorates astrocyte apoptosis after OGD injury.

Having established that low glucose markedly upregulates astrocytic BDH1, we used transcriptomics to probe the biological functions of astrocytic BDH1. siRNA was applied to silence BDH1 in vitro, and western blot confirmed that BDH1 was almost completely silenced at the 1022 position (Figure s6B), indicating successful knockdown in astrocytes. PCA of all transcribed genes clearly separated the two groups along the first principal component, with minimal overlap, reflecting inter-group differences and intra-group similarity (Fig. 5E). Volcano plot differential expression analysis (fold change > 1 or < -1, $P < 0.05$) identified 6,643 upregulated genes and 4,124 significantly downregulated genes in siBDH1 cells relative to siNC (Fig. 5F). A heatmap of key differentially expressed genes revealed marked downregulation of antioxidant genes such as cybb, slfn2, Ncf1, Hmox1, and sqstm1, along with induction of pro-apoptotic genes, including members of the caspase family and PRKDC (Fig. 5G). GO enrichment analysis indicated significant changes in mitochondrial outer membrane integrity and in intracellular oxidative stress homeostasis (Fig. 5H). In contrast, KEGG analysis highlighted significant alterations in glutathione homeostasis and apoptotic pathways (Fig. 5I). Silencing astrocytic BDH1 therefore produces a pronounced imbalance in oxidative stress, indicating that BDH1 plays a critical role in maintaining redox homeostasis in astrocytes.

To further validate these findings, siNC and siBDH1 cells were subjected to low-glucose stimulation followed by 4 h of OGD, after which ROS, MDA, and SOD levels were measured. ROS levels rose significantly after OGD injury (Fig. 5J); OGD + LG markedly suppressed this rise, and OGD + LG+siBDH1 abolished the protection afforded by low glucose. MDA levels followed a nearly identical pattern (Fig. 5K). SOD activity increased significantly with low-glucose stimulation compared with OGD alone but was significantly inhibited upon BDH1 knockdown (Fig. 5L). Together, these results demonstrate that, in the OGD model, low-glucose stimulation exerts antioxidant protection by activating BDH1.

Transcriptomic GO enrichment also highlighted significant changes in mitochondrial outer membrane and apoptotic pathways, prompting us to test whether altered BDH1 expression in astrocytes further worsens mitochondrial structural damage and apoptosis. Mitochondrial proteins were isolated successfully from astrocytes (Figure s6C), and a western blot of the mitochondrial fractions for the key apoptotic proteins caspase-3, Bax, and Bcl2 (Figure s6D) showed that the OGD + LG group had markedly reduced caspase-3 and Bax levels relative to the OGD group, an effect significantly reversed in the siBDH1 group. Immunofluorescence gave concordant results: the fluorescence intensity of Bax and caspase-3 colocalised with GFAP+TOM20 was significantly weaker in the OGD + LG group than in the OGD group but markedly stronger in the OGD + LG+siBDH1 group (Fig. 5M-N, Fig. 6E). These findings confirm that BDH1 knockdown profoundly disrupts redox homeostasis in astrocytes and, in turn, exacerbates mitochondria-mediated apoptosis.

To further evaluate the impact of BDH1 on mitochondrial function, we assessed mitochondrial membrane potential (ΔΨm) by JC-1 staining. Under normal conditions, JC-1 forms aggregates that emit red fluorescence; when mitochondrial structure and function are impaired, ΔΨm decreases, and JC-1 dissociates into monomers that emit green fluorescence. As shown in Fig. 5O-P, the OGD group exhibited a markedly increased proportion of monomeric JC-1 compared with the control group. Low-glucose stimulation significantly restored ΔΨm, as evidenced by an increased proportion of JC-1 aggregates, whereas the OGD + LG+siBDH1 group showed a further increase in the monomeric form. We next used transmission electron microscopy (TEM) to examine mitochondrial structural damage in neurons from mice subjected to I/R injury with eTRF and/or astrocytic BDH1 knockdown. As shown in Fig. 5Q, mitochondrial morphology in the eTRF + AAV-NC group was comparable to that in the A/L + AAV-NC group, although the eTRF + AAV-NC group contained a significantly higher number of mitochondria. In the eTRF + AAV-BDH1 group, mitochondria displayed prominent vacuolization and marked outer membrane damage. After I/R injury, the eTRF + AAV-NC group showed substantially less mitochondrial vacuolization and restored outer membrane integrity relative to the A/L + AAV-NC group, indicating that eTRF preconditioning strengthens the tolerance of neuronal mitochondria to I/R injury. This protection was, however, partially reversed in the eTRF + AAV-BDH1 group, in which mitochondria exhibited reduced matrix density and disorganised or disrupted cristae. These TEM data further confirm that eTRF significantly enhances neural mitochondrial tolerance to ischemia-reperfusion injury, an effect partially abolished by astrocytic BDH1 knockdown. Overall, our experiments provide robust evidence that, after OGD injury, BDH1 regulates both oxidative stress and mitochondrial dysfunction.

## 6. The Slfn2/Nrf2 Axis Mediates the Anti-Oxidative Stress and Anti-Mitochondrial Apoptosis Effects of BDH1

We next investigated the molecular mechanism by which BDH1 mediates anti-oxidative stress and mitochondrial apoptosis. Transcriptomic analysis revealed that BDH1 knockdown significantly reduced slfn2 expression. Recent work has shown that, in T cells, slfn2 binds transfer RNA (tRNA) directly and protects it from cleavage by the ribonuclease angiogenin, thereby attenuating ROS and oxidative stress

responses and sustaining the robust protein synthesis required for T cell expansion and immunity[26]. Nuclear factor erythroid 2-related factor 2 (Nrf2) is a well-established key transcription factor that regulates cellular anti-oxidative stress responses, and multiple studies have demonstrated that BDH1 plays an important role in activating NRF2[27]. To test whether BDH1 acts on oxidative stress through the slfn2/NRF2 pathway, we first asked whether manipulating BDH1 expression alters slfn2/NRF2 activation. As shown in Fig. 6A-B, the low-glucose stimulation group exhibited significantly increased slfn2 protein expression compared with the OGD group, whereas slfn2 expression was markedly suppressed after BDH1 knockdown. Western blot analysis of Nrf2 nuclear translocation showed that low-glucose stimulation promoted nuclear Nrf2 expression, and this effect was significantly inhibited by BDH1 knockdown. qPCR further confirmed these findings: low-glucose stimulation significantly increased slfn2 and Nrf2 mRNA levels, whereas BDH1 knockdown significantly suppressed their mRNA expression (Fig. 6C-D). We next examined the expression of the common antioxidant genes HO-1 and GCLC by qPCR. As shown in Fig. 6E-F, HO-1 and GCLC expression were significantly upregulated under low-glucose stimulation, and this upregulation was markedly inhibited by BDH1 knockdown. These results demonstrate that BDH1 is a key upstream molecule governing the antioxidant function of the slfn2/NRF2 axis.

To further determine whether slfn2 serves as the critical bridge mediating BDH1-dependent regulation of NRF2, we silenced slfn2 expression by siRNA (Figure s6F). As shown in Fig. 6G, western blot analysis demonstrated that, compared with the low-glucose stimulation group, slfn2 knockdown significantly reduced nuclear NRF2 expression and increased the levels of the mitochondrial apoptotic proteins Bax and caspase-3. In the double knockdown group (slfn2 and BDH1), nuclear NRF2 expression fell further, and the levels of mitochondrial apoptotic proteins rose further. These findings confirm that BDH1 regulates mitochondrial apoptosis through the slfn2/NRF2 pathway.

## 7. Semaglutide Partially Recapitulates the Neuroprotection of Time-Restricted Fasting After Cerebral Ischemia-Reperfusion Injury Through Glycemic Regulation

Our results identify the regulation of blood glucose levels as a key trigger of the neuroprotective mechanisms induced by Time-Restricted Fasting. This raised the question of whether drugs that act mainly on glucose control could reproduce such neuroprotection without dietary intervention. Semaglutide, a glucagon-like peptide-1 (GLP-1) receptor agonist expressed in multiple organs, including the brain, lowers blood glucose by upregulating glucagon levels[28]. It has also been reported to drive preferential utilisation of fat burning in neurons of the dorsal vagal complex (DVC) and to raise blood ketone levels[29], a mechanism closely resembling that of Time-Restricted Fasting. We therefore tested whether semaglutide administration confers neuroprotection after cerebral ischemia. Following published protocols, semaglutide was given for ten consecutive days (day 1: 15 μg/kg; day 2: 30 μg/kg; days 3–10: 60 μg/kg), as outlined in Fig. 7A. Body weight was monitored first (Fig. 7B): semaglutide alone produced no significant weight change relative to the control group, whereas combining

semaglutide with fasting resulted in a marked additional weight reduction compared with fasting alone, suggesting an additive effect on weight regulation. Random blood glucose monitoring (Fig. 7C) showed that eTRF mice had significantly lower and more stable glucose values than ad libitum-fed mice, confirming that eTRF effectively stabilises glucose homeostasis. Semaglutide alone also lowered blood glucose to some extent, with a clear decrease after each dose. Notably, mice receiving both eTRF and semaglutide exhibited pronounced glycemic fluctuations, with peaks following feeding and drug administration.

After these interventions, an I/R model was established in each group, and ischemic injury was assessed by TTC staining and neurobehavioral tests. TTC staining showed that eTRF alone and semaglutide alone each significantly reduced cerebral infarct size relative to the I/R group; surprisingly, infarct volume in the eTRF+semaglutide combination group was significantly larger than in either monotherapy group (Fig. 7D). In the open field test (Fig. 7E-H), each monotherapy significantly improved motor function relative to the I/R group, whereas the combination group travelled a significantly shorter total distance than either monotherapy group. The mNSS results (Figure s6G) were consistent with these findings. Both monotherapies significantly reduced mNSS scores relative to the I/R group, whereas the combination group had significantly higher mNSS scores than either monotherapy group. Finally, TUNEL staining co-localised with GFAP and MAP2 was used to evaluate neuronal and astrocytic apoptosis (Fig. 7I-J). eTRF alone significantly reduced post-I/R apoptosis in both neurons and astrocytes compared with the I/R group, whereas semaglutide alone or the combination resulted in higher apoptosis levels than eTRF monotherapy.

To clarify how semaglutide affects I/R injury, we measured serum β-hydroxybutyrate. We confirmed that semaglutide enhanced its synthesis in vivo, whereas combining semaglutide with intermittent fasting suppressed endogenous β-hydroxybutyrate production (Fig. 7K). The effects of semaglutide on astrocyte apoptosis and NRF2 signalling were then assessed in vitro. As shown in Fig. 7L-O, LG and semaglutide each significantly alleviated apoptosis relative to the OGD group, with LG being the most effective; when LG and semaglutide were combined, apoptosis returned to levels comparable to those in the OGD group. Mechanistically, semaglutide alone activated the NRF2 pathway, but no significant change occurred in the LG+semaglutide combination group. These results indicate that semaglutide alone is neuroprotective after stroke, whereas its combination with Time-Restricted Fasting largely diminishes the benefits of fasting alone.

# Discussion

Although dietary interventions have been recommended in recent years as a primary measure for preventing cerebral ischemia, how time-restricted feeding (TRF) promotes post-stroke neural repair remains poorly understood. Using a mouse model of cerebral ischemia-reperfusion (I/R) injury, this study systematically demonstrated for the first time that early time-restricted feeding (eTRF) can significantly alleviate brain injury and improve neurological function by inducing glycolipid metabolic reprogramming in the nervous system. We further identified BDH1, a key enzyme involved in ketone body metabolism in

astrocytes, as a core molecular target mediating the protective effects of eTRF: BDH1 acts through the slfn2/NRF2 antioxidant axis to alleviate oxidative stress and mitochondrial apoptosis. These findings reveal a novel mechanism by which circadian dietary intervention confers neuroprotection through metabolic reprogramming and provide a non-invasive, highly compliant adjunctive therapeutic strategy for cerebral ischemia.

Following cerebral ischemia-reperfusion injury, disruption of metabolic homeostasis in the nervous system is a core pathophysiological basis underlying neurological dysfunction and brain tissue damage [30]. During ischemia, hypoxia and glucose deprivation rapidly deplete ATP in neural cells and impair mitochondrial oxidative phosphorylation, thereby triggering a burst of oxidative stress and mitochondrial apoptosis upon reperfusion [31, 32]. Therefore, restoring metabolic homeostasis after cerebral ischemia-reperfusion injury is crucial. However, previous studies have mostly examined individual metabolic pathways in isolation, lacking a systematic analysis of dynamic, cell-type-specific changes. By integrating bulk and single-cell transcriptomic data, we reveal for the first time the temporal changes in metabolic pathways after stroke: glycolysis undergoes compensatory upregulation during the acute phase, while oxidative phosphorylation and fatty acid oxidation gradually recover during the recovery phase. Notably, astrocytes and microglia exhibit markedly distinct patterns of metabolic adaptation: the former are characterised by sustained suppression of aerobic metabolism, whereas the latter display classical immunometabolic activation.

Clinical trials in patients with type 2 diabetes have shown that early time-restricted feeding (eTRF)—20-hour fasting on three nonconsecutive days per week—can significantly improve glucose tolerance [33]. Intermittent fasting may also enhance lipolysis, insulin sensitivity, and adipose tissue remodelling, while restoring gut microbiota diversity [34]. The benefits of eTRF in central nervous system disorders have likewise attracted increasing attention [35, 36]. In this study, we systematically investigated how eTRF affects neuronal glucose and lipid metabolic homeostasis following cerebral ischemia by measuring the expression of genes involved in glucose and lipid metabolism in eTRF-treated mice and by performing metabolomic sequencing. We found that eTRF altered the utilisation of energy substrates in the nervous system. Although the upregulation of fatty acids did not directly increase ATP production, changes in acetyl-CoA (Acetyl-CoA) levels drew our particular attention. Acetyl-CoA, which is known to be generated through fatty acid breakdown, can either enter the tricarboxylic acid cycle to supply ATP or enter the ketone body metabolic pathway. By measuring serum β-hydroxybutyrate and the ketogenesis-related genes Scot, Acat1, and Bdh1, we confirmed that the upregulation of acetyl-CoA increased the level of ketone body production. In conclusion, we demonstrated for the first time that eTRF can induce alterations in glucose and lipid metabolic homeostasis after cerebral ischemia and reprogram these metabolic pathways toward ketone body metabolism.

Astrocytes are the most abundant glial cells in the central nervous system and are core regulators of brain metabolic homeostasis. Their endfoot structures form the neurovascular unit, linking blood vessels to neurons and delivering blood-derived glucose to sustain neuronal activity[37, 38]. When neuronal activity surges or blood glucose levels decline, astrocytes rapidly break down glycogen into lactate,

providing neurons with an efficient energy substrate through the well-known “lactate shuttle”. We found that eTRF, a dietary intervention, significantly alleviated lactate accumulation following cerebral ischemia/reperfusion (I/R) injury, most likely by markedly stabilising blood glucose homeostasis. It has been reported that astrocytes are the only cells in the nervous system with a complete lipid oxidation system, enabling them to support neural energy supply through ketone body production. This prompted us to investigate whether BDH1, a key enzyme involved in ketone body synthesis in astrocytes, is a critical target through which eTRF triggers metabolic regulation following cerebral I/R injury. In vivo experiments showed that AAV (adeno-associated virus)-mediated targeted knockdown of BDH1 in astrocytes significantly reversed the neuroprotective effects mediated by eTRF following cerebral I/R injury. This key role of astrocytic BDH1 in eTRF was subsequently validated in vitro. Because blood glucose levels were significantly reduced under the eTRF diet, we simulated the fasting metabolic state of astrocytes by lowering the glucose concentration under serum-free conditions; measurements of glucose and lipid transporters, as well as BDH1, confirmed that this model was metabolically synchronised with eTRF in vivo. Transcriptomic analysis identified BDH1 as a key mediator regulated by oxidative stress: low-glucose treatment significantly increased reactive oxygen species (ROS) and malondialdehyde (MDA) levels, as well as superoxide dismutase (SOD) activity, while BDH1 knockdown further exacerbated oxidative stress-induced damage. GO enrichment analysis revealed significant changes in the mitochondrial outer membrane following BDH1 inhibition, a finding also confirmed by our experiments: knocking down BDH1 in astrocytes aggravated mitochondrial outer membrane damage, and silencing BDH1 further exacerbated mitochondrial apoptosis. Therefore, in addition to serving as a key ketogenic enzyme, BDH1 also contributes to eTRF-mediated protection against cerebral ischemia/reperfusion (I/R) injury by regulating oxidative stress and mitochondrial damage.

Post-stroke oxidative stress is one of the core pathological mechanisms triggering secondary brain injury. Excessive production of reactive oxygen species (ROS), coupled with insufficient clearance, disrupts the oxidant-antioxidant balance and causes extensive damage to brain cells and blood vessels. Consistent with previous reports, we confirmed that numerous antioxidant genes were significantly downregulated following BDH1 knockdown. At the same time, GO enrichment analysis revealed marked alterations in oxidative stress responses and intracellular oxygen homeostasis pathways. Among these genes, slfn2 exhibited the most pronounced change and serves as a key regulator of antioxidant activity. slfn2 is essential for protecting T cells from oxidative stress-induced damage and maintaining their immune function; moreover, mice carrying slfn2 mutations are more susceptible to bacterial and viral infections, and exhibit increased endogenous T-cell apoptosis following T-cell receptor (TCR) stimulation and interleukin-7 (IL-7) signalling [39]. Therefore, we further investigated whether slfn2, a key cytoplasmic protein that regulates oxidative stress homeostasis, mediates the nuclear translocation of the transcription factor NRF2, which is activated by the mitochondria-associated protein BDH1. Our data show that the combination of low-sugar stimulation and siRNA-mediated regulation of BDH1 expression significantly altered the nuclear translocation of SLFN2 and NRF2. At the same time, the transcriptional activation of antioxidant genes, including heme oxygenase-1 (HO-1) and glutathione peroxidase-like

protein (GCLC), was also tightly controlled by BDH1. These data indicate that the SLFN2/NRF2 signalling pathway is a key mechanism by which BDH1 regulates oxidative stress and mitochondrial apoptosis.

The circadian rhythm-regulated form of Time-Restricted Fasting (TRF)—early Time-Restricted Feeding (eTRF)—is widely recognised for its significant benefits in diabetes prevention and treatment, as well as weight management [40, 41]. In addition to affecting ketone metabolism, eTRF can activate glucagon-like peptide-1 (GLP-1) in the gastrointestinal tract, thereby alleviating high-fat diet-induced intestinal inflammation[42]. The novel GLP-1 agonist, semaglutide, has been shown to regulate glucose homeostasis by increasing glucagon secretion and has demonstrated significant efficacy in diabetes treatment and weight management [43, 44]. Previous studies have reported that semaglutide plays an important role in regulating fatty acid and ketone body metabolism in neurons [29], a finding that appears closely associated with the metabolic changes induced by eTRF stimulation. Therefore, we investigated whether semaglutide could exert protective effects similar to those of eTRF through a pharmacological alternative pathway following cerebral ischemia/reperfusion (I/R) injury, as well as the effects of combining semaglutide with eTRF on cerebral I/R injury. In measurements of body weight and random blood glucose, mice administered semaglutide continuously for 10 days did not show a significant decrease in body weight; however, their random blood glucose levels were generally lower than those of the A/L+NaCl group, with levels reaching a low point after each semaglutide administration. Mice receiving eTRF alone showed a slight decrease in body weight, a significant reduction in blood glucose, and generally stable fluctuations in blood glucose levels. Concurrent measurement of serum β-hydroxybutyrate levels further confirmed that semaglutide significantly promoted ketogenesis in vivo. These results indicate that long-term regulation of blood glucose through eTRF can achieve a healthier metabolic state. Subsequently, we evaluated I/R injury in mice from different groups using behavioural tests, triphenyltetrazolium chloride (TTC) staining, and the terminal deoxynucleotidyl transferase-mediated dUTP nick-end labelling (TUNEL) assay. Our results confirmed that both eTRF and semaglutide significantly ameliorated I/R injury in mice. Interestingly, in the group receiving combined semaglutide + eTRF treatment, body weight decreased significantly during semaglutide administration; more importantly, random blood glucose measurements revealed pronounced fluctuations in glycemic control, indicating a substantial impact on glucose regulation. Moreover, the recovery of I/R injury in these mice was markedly weaker than that observed in the groups treated with eTRF or semaglutide alone. Our findings further support the existing view that dysregulated glucose metabolism is a key factor exacerbating cerebral ischemic injury, possibly because the combined use of semaglutide and eTRF leads to a severe imbalance in the regulation of oxidative stress and mitochondrial apoptosis. Overall, our data indicate that combined eTRF and semaglutide treatment can accelerate weight loss, but long-term use may disrupt glucose homeostasis and aggravate cerebral I/R injury.

It should be acknowledged that this study has several limitations. First, because of the difficulty in obtaining human samples, all experiments relied on animal models. Second, although our study clearly demonstrated significant alterations in glycolipid metabolism in the nervous system, we did not investigate in depth the specific metabolic changes in glucose or fatty acids, partly because the marked

alterations in ketone body signalling pathways attracted our primary attention. Third, our results clearly indicate that SLFN2 is a key regulator mediating BDH1-mediated regulation of NRF2; however, the precise mode of interaction among these proteins has not yet been directly validated. Further studies will help to fully elucidate the regulatory role of the SLFN2/NRF2 axis in oxidative stress.

# Conclusion

In summary, this study clarifies the protective role of eTRF in cerebral I/R injury. eTRF activates astrocytic BDH1 by regulating metabolic reprogramming processes in the nervous system and ameliorates oxidative stress and mitochondrial apoptosis through the slfn2/NRF2 pathway. In addition, we confirmed that semaglutide also exerts a neuroprotective effect in cerebral I/R injury.

# Declarations


### Acknowledgements

Not applicable.

### Funding sources

This research was funded by the National Natural Science Foundation of China (NSFC) (82101409), NSFC (32071036), and the Natural Science Foundation of Heilongjiang Province (No. LH2023H028) Heilongjiang Province Science and Technology Innovation Base Project (No. JD24D004)


### Conflicts of interest

The author declares no conflicts of interest.

### Author contributions

H.Y., YY.Z.: conceptualization,writing-original draft, methodology, visualization. HY.Z., DD.W., H.C.: resources, literature survey. K.L., XM.Z, H.Y., Q.Y.: literature survey,methodology, visualization. JR.W., SS.Y: supervision, funding acquisition. G.W., T.Z.: supervision, writing-review and editing, funding acquisition. The authors declare that they have not use AI-generated work in this manuscript.

### Availability of data and materials

The supporting data for the results of this study can be provided upon reasonable request from the corresponding author, T.Z. Additionally, all supplementary files are included in the original manuscript.

### Ethical approval and consent to participate

All experimental protocols and procedures were approved by the Institutional Animal Care and Use Committee of Harbin Medical University and were carried out in accordance with the guidelines for the

care and use of laboratory animals of the National Institutes of Health of the United States. All authors agreed to the final version and to submit the manuscript to this journal.

**Clinical trial number**

Not applicable.

**Consent to publish**

All participants obtained written informed consent for publication.

**Author details**

Department of Neurobiology, School of Basic Medical Sciences, Harbin Medical University, Harbin 150081, Heilongjiang Province.

# References

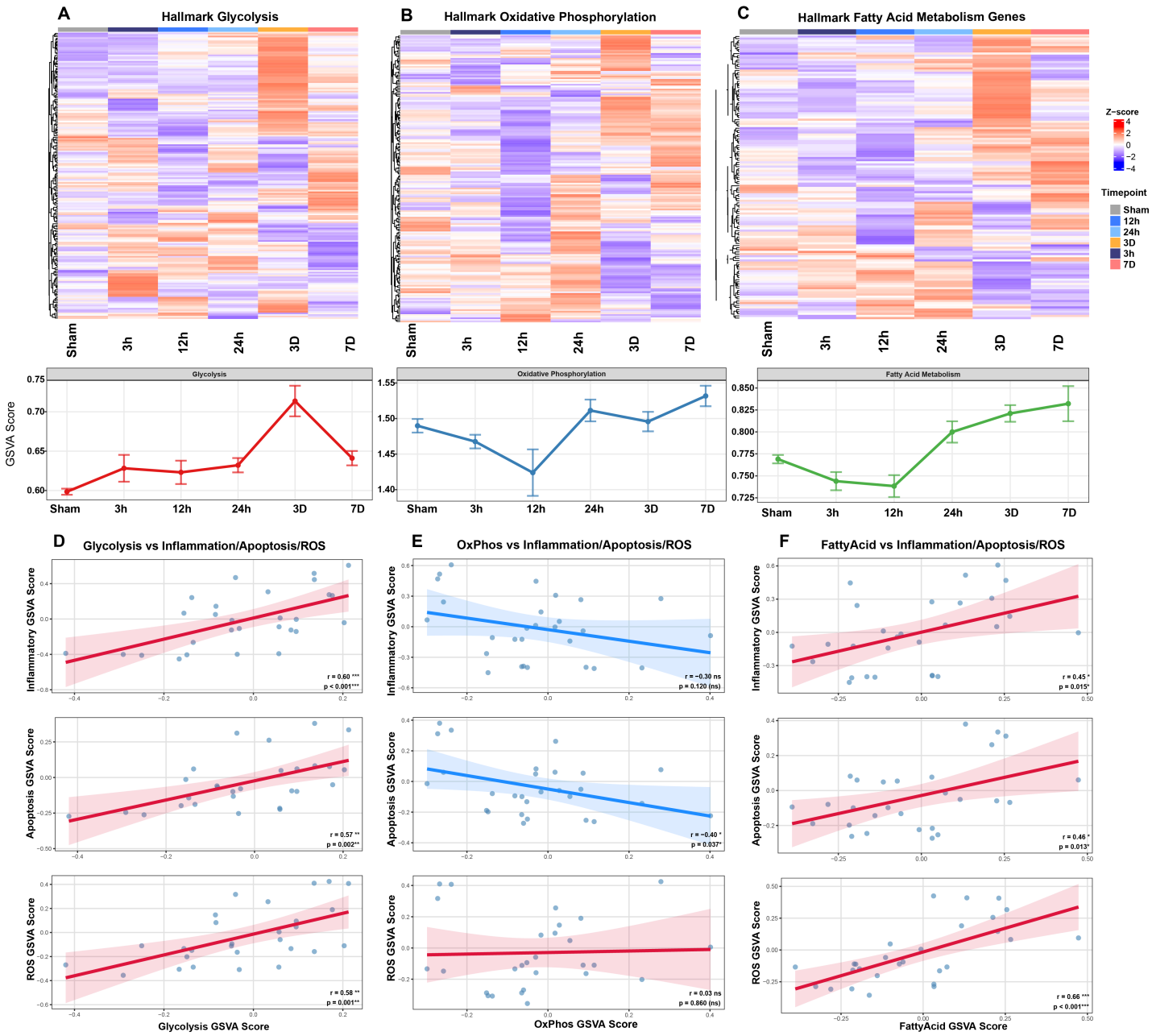
1. Wang Y, Ge M, Wang J, et al. Metabolic reprogramming in ischemic stroke: when glycolytic overdrive meets lipid storm[J]. Cell Death Dis, 2025, 16(1): 788. DOI:10.1038/s41419-025-08114-w.
2. An H, Zhou B, Ji X. Mitochondrial quality control in acute ischemic stroke[J]. J Cereb Blood Flow Metab, 2021, 41(12): 3157–3170. DOI:10.1177/0271678X211046992.
3. Zhu M, Cao L, Xiong S, et al. Na(+)/K(+)-ATPase-dependent autophagy protects brain against ischemic injury[J]. Signal Transduct Target Ther, 2020, 5(1): 55. DOI:10.1038/s41392-020-0153-7.
4. Li Y W, Liu Y, Luo S Z, et al. The significance of calcium ions in ischemic stroke-reperfusion injury: mechanisms and intervention strategies[J]. Front Mol Biosci, 2025, 12: 1585758. DOI:10.3389/fmolb.2025.1585758.
5. Zhang C, Lan X, Wang Q, et al. Decoding ischemic stroke: Perspectives on the endoplasmic reticulum, mitochondria, and their crosstalk[J]. Redox Biol, 2025, 82: 103622. DOI:10.1016/j.redox.2025.103622.
6. Ho J P, Powers W J. Contemporary Management of Acute ischemic stroke[J]. Annu Rev Med, 2025, 76(1): 417–429. DOI:10.1146/annurev-med-050823-094312.
7. Geisler C E, Hepler C, Higgins M R, et al. Hepatic adaptations to maintain metabolic homeostasis in response to fasting and refeeding in mice[J]. Nutr Metab (Lond), 2016, 13: 62. DOI:10.1186/s12986-016-0122-x.
8. Loren Y, Norman G, Veronica J. The acute effect of time-restricted feeding (12 & 16 h) and varying exercise intensities on fat-oxidation rate in inactive young adults - a randomized control trial[J]. BMC Sports Sci Med Rehabil, 2024, 16(1): 169. DOI:10.1186/s13102-024-00959-6.
9. Liu Y, Cheng A, Li Y J, et al. SIRT3 mediates hippocampal synaptic adaptations to intermittent fasting and ameliorates deficits in APP mutant mice[J]. Nat Commun, 2019, 10(1): 1886. DOI:10.1038/s41467-019-09897-1.

10. Jeong S, Chokkalla A K, Davis C K, et al. Circadian-Dependent Intermittent Fasting Influences Ischemic Tolerance and Dendritic Spine Remodeling[J]. Stroke, 2024, 55(8): 2139–2150. DOI:10.1161/STROKEAHA.124.046400.
11. Vasconcelos A R, Yshii L M, Viel T A, et al. Intermittent fasting attenuates lipopolysaccharide-induced neuroinflammation and memory impairment[J]. J Neuroinflammation, 2014, 11: 85. DOI:10.1186/1742-2094-11-85.
12. Dembitskaya Y, Piette C, Perez S, et al. Lactate supply overtakes glucose when neural computational and cognitive loads scale up[J]. Proc Natl Acad Sci U S A, 2022, 119(47): e2212004119. DOI:10.1073/pnas.2212004119.
13. Silva B, Mantha O L, Schor J, et al. Glia fuel neurons with locally synthesized ketone bodies to sustain memory under starvation[J]. Nat Metab, 2022, 4(2): 213–224. DOI:10.1038/s42255-022-00528-6.
14. Andersen J V, Westi E W, Jakobsen E, et al. Astrocyte metabolism of the medium-chain fatty acids octanoic acid and decanoic acid promotes GABA synthesis in neurons via elevated glutamine supply[J]. Mol Brain, 2021, 14(1): 132. DOI:10.1186/s13041-021-00842-2.
15. Xu B T, Wan S R, Wu Q, et al. BDH1 overexpression alleviates diabetic cardiomyopathy through inhibiting H3K9bhb-mediated transcriptional activation of LCN2[J]. Cardiovasc Diabetol, 2025, 24(1): 101. DOI:10.1186/s12933-025-02646-3.
16. Ma X, Wang Z, Gao H, et al. beta-Hydroxybutyrate dehydrogenase 1: A promising therapeutic target for diverse diseases[J]. Biochem Pharmacol, 2025, 239: 117070. DOI:10.1016/j.bcp.2025.117070.
17. Oswald B M, Decamp L M, Longo J, et al. Dietary restriction reprograms CD8(+) T cell fate to enhance anti-tumour immunity and immunotherapy responses[J]. Nat Metab, 2025, 7(12): 2489–2509. DOI:10.1038/s42255-025-01415-6.
18. Otsuka H, Kimura T, Ago Y, et al. Deficiency of 3-hydroxybutyrate dehydrogenase (BDH1) in mice causes low ketone body levels and fatty liver during fasting[J]. J Inherit Metab Dis, 2020, 43(5): 960–968. DOI:10.1002/jimd.12243.
19. Wei X, Zhang C, Zheng X, et al. beta-hydroxybutyrate dehydrogenase promotes pancreatic cancer cell proliferation through regulation of the NAD(+)/NADH balance and mitochondrial acetylation[J]. J Biol Chem, 2025, 301(10): 110636. DOI:10.1016/j.jbc.2025.110636.
20. Wan S R, Teng F Y, Fan W, et al. BDH1-mediated betaOHB metabolism ameliorates diabetic kidney disease by activation of NRF2-mediated antioxidative pathway[J]. Aging (Albany NY), 2023, 15(22): 13384–13410. DOI:10.18632/aging.205248.
21. Chiang T, Messing R O, Chou W H. Mouse model of middle cerebral artery occlusion[J]. J Vis Exp, 2011(48). DOI:10.3791/2761.
22. Sun F, Zhou J, Chen X, et al. No-reflow after recanalization in ischemic stroke: From pathomechanisms to therapeutic strategies[J]. J Cereb Blood Flow Metab, 2024, 44(6): 857–880. DOI:10.1177/0271678X241237159.

23. Shi M Y, Yu H C, Han C Y, et al. p21-activated kinase 4 suppresses fatty acid beta-oxidation and ketogenesis by phosphorylating NCoR1[J]. Nat Commun, 2023, 14(1): 4987. DOI:10.1038/s41467-023-40597-z.
24. Morris G, Maes M, Berk M, et al. Nutritional ketosis as an intervention to relieve astrogliosis: Possible therapeutic applications in the treatment of neurodegenerative and neuroprogressive disorders[J]. Eur Psychiatry, 2020, 63(1): e8. DOI:10.1192/j.eurpsy.2019.13.
25. Li M, Wang Y, Wei X, et al. AMPK targets PDZD8 to trigger carbon source shift from glucose to glutamine[J]. Cell Res, 2024, 34(10): 683–706. DOI:10.1038/s41422-024-00985-6.
26. Yue T, Zhan X, Zhang D, et al. SLFN2 protection of tRNAs from stress-induced cleavage is essential for T cell-mediated immunity[J]. Science, 2021, 372(6543). DOI:10.1126/science.aba4220.
27. Xu B T, Teng F Y, Wu Q, et al. Bdh1 overexpression ameliorates hepatic injury by activation of Nrf2 in a MAFLD mouse model[J]. Cell Death Discov, 2022, 8(1): 49. DOI:10.1038/s41420-022-00840-w.
28. Zhang Y, Parajuli K R, Fava G E, et al. GLP-1 Receptor in Pancreatic alpha-Cells Regulates Glucagon Secretion in a Glucose-Dependent Bidirectional Manner[J]. Diabetes, 2019, 68(1): 34–44. DOI:10.2337/db18-0317.
29. Teixidor-Deulofeu J, Blid Skoldheden S, Font-Girones F, et al. Semaglutide effects on energy balance are mediated by Adcyap1(+) neurons in the dorsal vagal complex[J]. Cell Metab, 2025, 37(7): 1530–1546 e6. DOI:10.1016/j.cmet.2025.04.018.
30. Lei W, Zhuang H, Huang W, et al. Neuroinflammation and energy metabolism: a dual perspective on ischemic stroke[J]. J Transl Med, 2025, 23(1): 413. DOI:10.1186/s12967-025-06440-3.
31. Yuan Y, Tian Y, Jiang H, et al. Mechanism of PGC-1alpha-mediated mitochondrial biogenesis in ischemic stroke-reperfusion injury[J]. Front Mol Neurosci, 2023, 16: 1224964. DOI:10.3389/fnmol.2023.1224964.
32. D'apolito E, Sisalli M J, Tufano M, et al. Oxidative Metabolism in Brain Ischemia and Preconditioning: Two Sides of the Same Coin[J]. Antioxidants (Basel), 2024, 13(5). DOI:10.3390/antiox13050547.
33. Teong X T, Liu K, Vincent A D, et al. Intermittent fasting plus early time-restricted eating versus calorie restriction and standard care in adults at risk of type 2 diabetes: a randomized controlled trial[J]. Nat Med, 2023, 29(4): 963–972. DOI:10.1038/s41591-023-02287-7.
34. Silverii G A, Turrini A. Do We Just Need To Eat Less Often? An Update on the Role of Eating Frequency and Intermittent Fasting for Obesity Prevention and Management[J]. Curr Obes Rep, 2025, 14(1): 77. DOI:10.1007/s13679-025-00663-7.
35. Liu Z, Zhang J, Jiang F, et al. Biological Effects of Dietary Restriction on Alzheimer's Disease: Experimental and Clinical Investigations[J]. CNS Neurosci Ther, 2025, 31(4): e70392. DOI:10.1111/cns.70392.
36. Garber D, Pathan M, Eechampati A, et al. The Preclinical Effects of Prolonged Intermittent Fasting in an Animal Model on the Development of Multiple Sclerosis Pathology[J]. Cureus, 2025, 17(8): e91260. DOI:10.7759/cureus.91260.

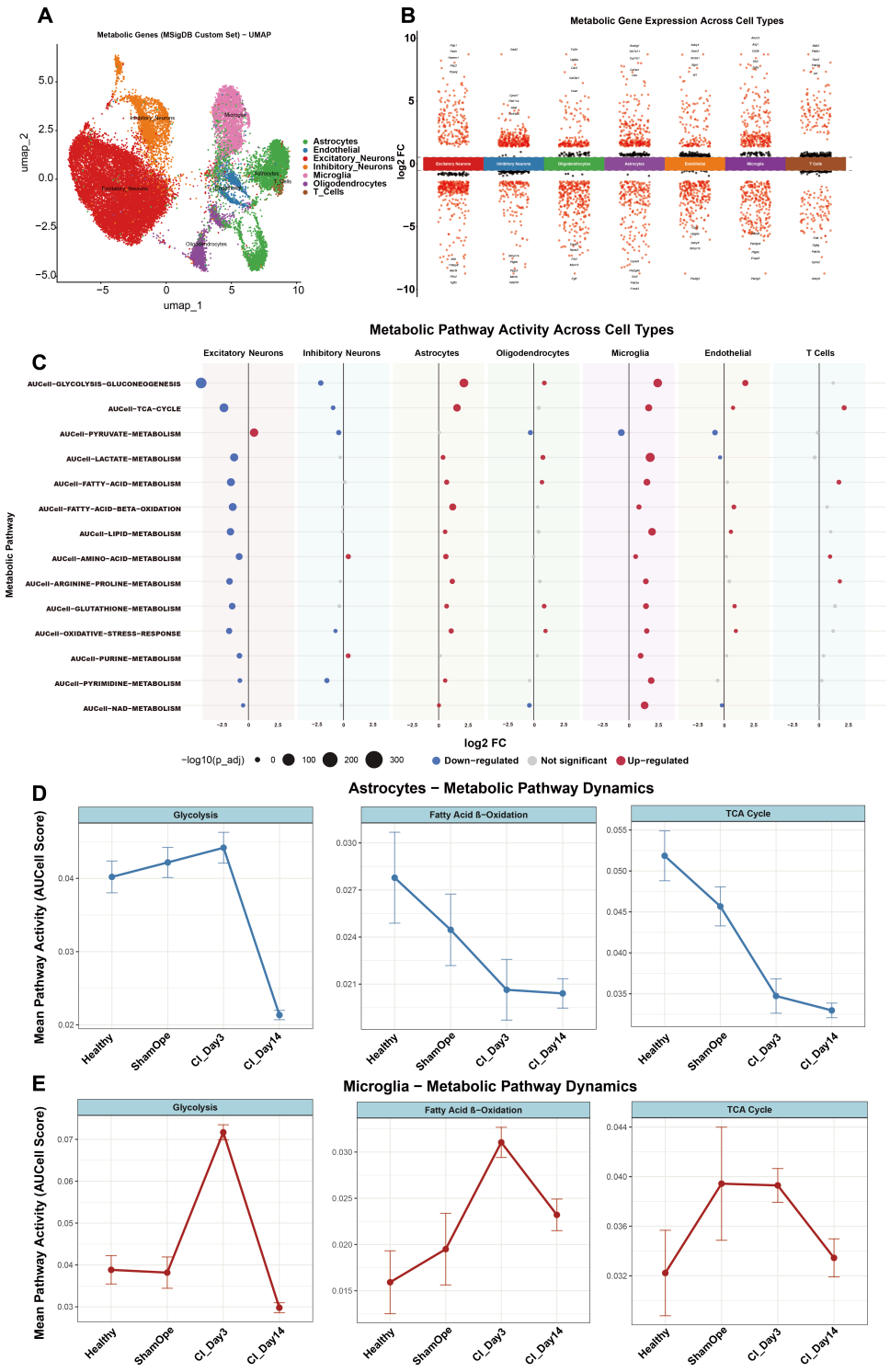
37. Beard E, Lengacher S, Dias S, et al. Astrocytes as Key Regulators of Brain Energy Metabolism: New Therapeutic Perspectives[J]. Front Physiol, 2021, 12: 825816. DOI:10.3389/fphys.2021.825816.
38. Diaz-Castro B, Robel S, Mishra A. Astrocyte Endfeet in Brain Function and Pathology: Open Questions[J]. Annu Rev Neurosci, 2023, 46: 101–121. DOI:10.1146/annurev-neuro-091922-031205.
39. Berger M, Krebs P, Crozat K, et al. An Slfn2 mutation causes lymphoid and myeloid immunodeficiency due to loss of immune cell quiescence[J]. Nat Immunol, 2010, 11(4): 335–43. DOI:10.1038/ni.1847.
40. Ezpeleta M, Cienfuegos S, Lin S, et al. Time-restricted eating: Watching the clock to treat obesity[J]. Cell Metab, 2024, 36(2): 301–314. DOI:10.1016/j.cmet.2023.12.004.
41. Anasanti M D, Hamzah N. Meta-analysis and meta-regression of intermittent fasting effects on glycaemic control in type 2 diabetes: Subgroup analyses and variability[J]. Diabetes Metab Syndr, 2025, 19(7): 103279. DOI:10.1016/j.dsx.2025.103279.
42. Eraky S M, Ramadan N M, Atif H M, et al. The ameliorating effect of intermittent fasting on intestinal glucagon-like peptide 1 in rats fed a high-fat diet via the Farnesoid X receptor and the Melanocortin-4 receptor[J]. Life Sci, 2025, 361: 123327. DOI:10.1016/j.lfs.2024.123327.
43. Papakonstantinou I, Tsioufis K, Katsi V. Spotlight on the Mechanism of Action of Semaglutide[J]. Curr Issues Mol Biol, 2024, 46(12): 14514–14541. DOI:10.3390/cimb46120872.
44. Frias J P, Auerbach P, Bajaj H S, et al. Efficacy and safety of once-weekly Semaglutide 2.0 mg versus 1.0 mg in patients with type 2 diabetes (SUSTAIN FORTE): a double-blind, randomised, phase 3B trial[J]. Lancet Diabetes Endocrinol, 2021, 9(9): 563–574. DOI:10.1016/S2213-8587(21)00174-1.

# Figures




## Figure 1

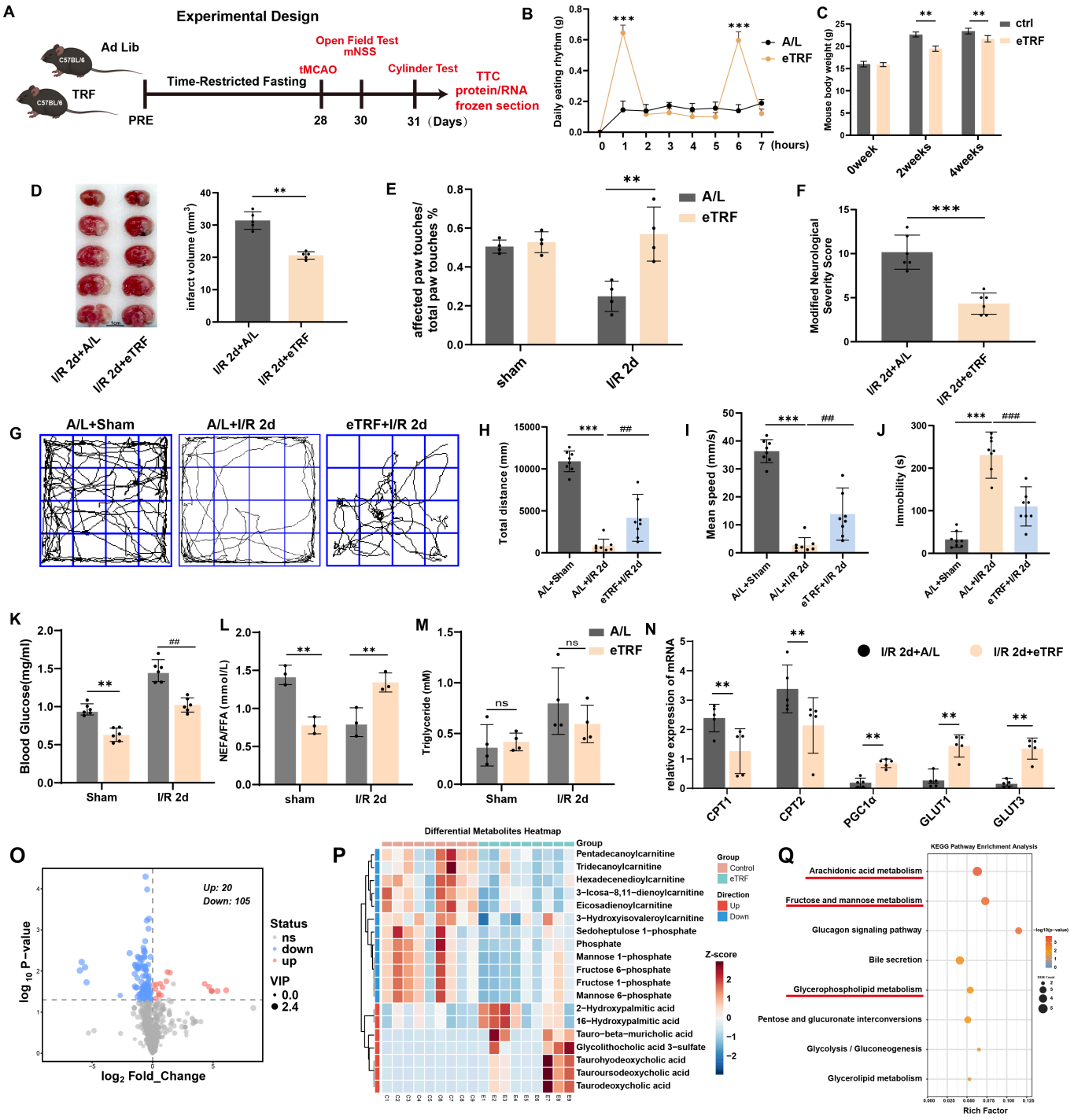
Bulk transcriptomic profiling reveals temporal metabolic reprogramming and its pathological correlates after ischemic stroke. (A–C) Heatmaps and line plots depicting the expression dynamics of glycolysis (A), oxidative phosphorylation (B), and fatty acid metabolism (C) pathway genes at 3 h, 12 h, 24 h, 3 d, and 7 d post-stroke, based on MSigDB gene sets. (D–F) Pearson correlation heatmaps showing the relationships between the activity scores of glycolysis (D), oxidative phosphorylation (E), and fatty acid metabolism (F) and the pathway scores for inflammation, apoptosis, and reactive oxygen species (ROS).




## Figure 2

Single-nucleus RNA-seq uncovers cell-type-specific metabolic reprogramming after cerebral ischemia. (A) UMAP visualization of a global metabolic activity score, calculated as the mean expression of 1,595 MSigDB metabolic genes per cell. (B) Scatter plot of differentially expressed metabolic genes across seven identified cell types, illustrating distinct metabolic transcriptional profiles. (C) Dot plot integrating

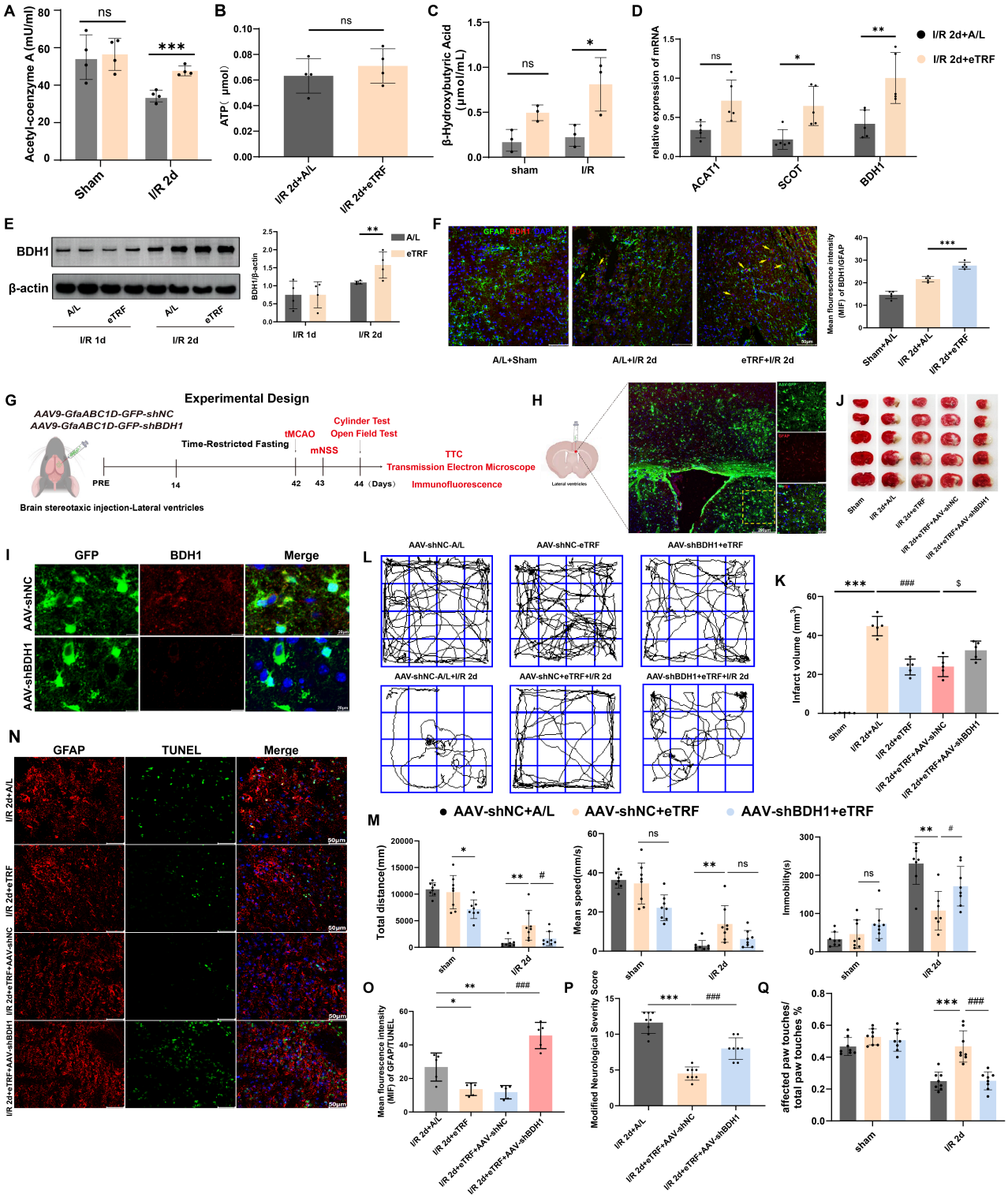
the enrichment of 28 MSigDB metabolic pathways across cell types. (D-E) AUCell-based pathway activity scores for glycolysis, the TCA cycle, and fatty acid β-oxidationin astrocyte and microglia.




## Figure 3

Early Time-Restricted Fasting alleviates cerebral ischemia-reperfusion injury and remodels systemic and neural metabolic homeostasis.

(A) Experimental design and treatment flowchart for C57BL/6 mice subjected to ad libitum (A/L) or early time-restricted fasting (eTRF) and I/R surgery. (B) Feeding rhythm of mice over 24 h, showing the temporal distribution of food intake. (n = 8). (C) Body weight changes after 2 and 4 weeks of dietary intervention. (n = 8). (D) Representative TTC-stained brain sections and quantification of cerebral infarct volume in A/L and eTRF mice after I/R. (n = 5). (E) Cylinder test assessing forelimb use asymmetry. (n = 4). (F) Modified neurological severity score (mNSS) evaluating neurological deficits. (n = 6). (G) Representative locomotor trajectories in the open field test. (H-J) Quantification of total distance traveled (H), mean speed (I), and immobility time (J) during the open field test.(n = 8). (K-M) Serum levels of glucose (K), non-esterified fatty acids (NEFA) (L), and triglycerides (TG) (M) in sham and I/R mice under A/L or eTRF conditions.(n = 3-6). (N) Relative mRNA expression of Cpt1, Cpt2, and Glut3 in the ischemic brain of A/L and eTRF mice after I/R, determined by qPCR. (n = 5). (O) Volcano plot of metabolomic profiling from the ipsilateral cortex of I/R mice treated with eTRF versus A/L, identifying 125 differential metabolites. (P) Heatmap illustrating changes in glucose and lipid metabolism-related metabolites following eTRF intervention. (Q) KEGG pathway enrichment analysis of significantly altered metabolic pathways, including fructose and mannose metabolism, glycolysis/gluconeogenesis, arachidonic acid metabolism, and glycerophospholipid metabolism. $^{**}P<0.01$; $^{***}P<0.001$;$^{\#\#}P<0.01$; $^{\#\#\#}P<0.001$ Mean±SEM, T-test,One-way ANOWA, Two-way ANOWA.

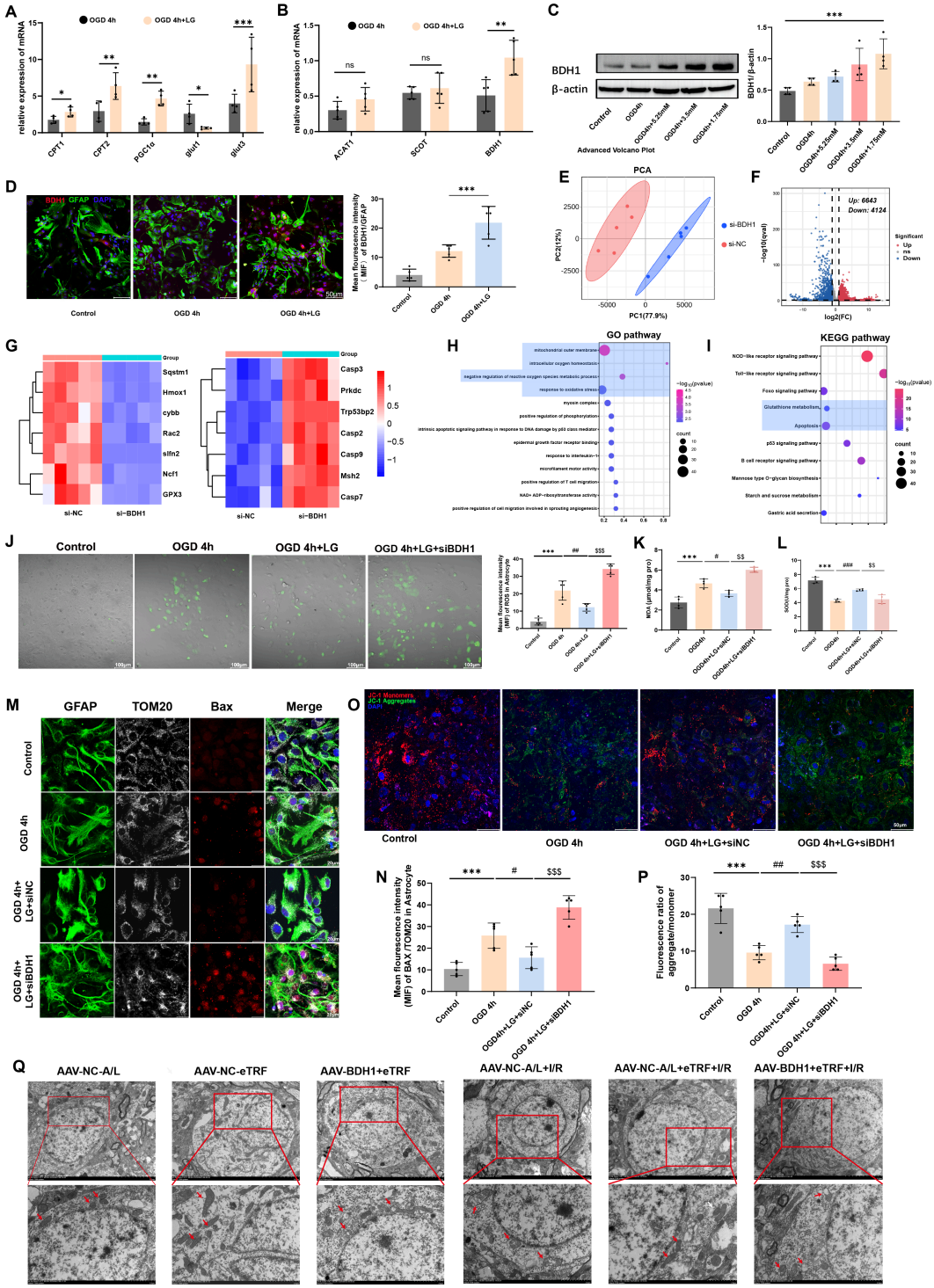



## Figure 4

Astrocytic BDH1 is a critical metabolic target of eTRF in ameliorating cerebral ischemia–reperfusion injury.

(A) Acetyl-CoA synthetase activity in the brain of A/L and eTRF mice under physiological conditions and after I/R injury. (n = 4). (B) ATP levels in the ischemic brain of A/L and eTRF mice after I/R. (n = 4). (C)

Serum β-hydroxybutyrate levels in sham and I/R mice under A/L or eTRF treatment. (n = 3). (D) Relative mRNA expression of BDH1 in the brain of A/L and eTRF mice under physiological and post-I/R conditions. (n = 5). (E) Representative western blot and quantification of BDH1 protein levels in the ischemic brain of A/L and eTRF mice at 2 days post-I/R. (n = 4). (F) Immunofluorescence co-staining for BDH1 (red) and GFAP (green) in the peri-infarct cortex, with quantification of BDH1 fluorescence intensity in $GFAP^+$ astrocytes. Scale bar:50 μm. (n = 5). (G) Schematic timeline of AAV9-GFAP-shBDH1-GFP stereotaxic injection, eTRF intervention, and I/R surgery. (H) Representative immunofluorescence images showing co-localization of AAV-encoded GFP with GFAP in the injected hemisphere. bar: 200 μm. (I) Quantification of $GFP^+GFAP^+$ cells confirming astrocyte-specific transduction .bar: 20 μm. (J) Representative TTC-stained brain sections . (K) Quantification of infarct volume. (n = 5) (L-M) Open field test performance: total distance ;mean speed and immobility (n = 8). (N) TUNEL staining of peri-infarct cortical sections. (O) Quantification of TUNEL-positive cells. (n = 5). (P) mNSS evaluation of neurological function.(n = 8) (Q) Cylinder test for forelimb use asymmetry. (n = 8) $^{\#}P<0.05$; $^{*}P<0.05$; $^{**}P<0.01$; $^{***}P<0.001$;$^{\#\#}P<0.01$; $^{\#\#\#}P<0.001$ Mean±SEM, T-test,One-way ANOWA, Two-way ANOWA.

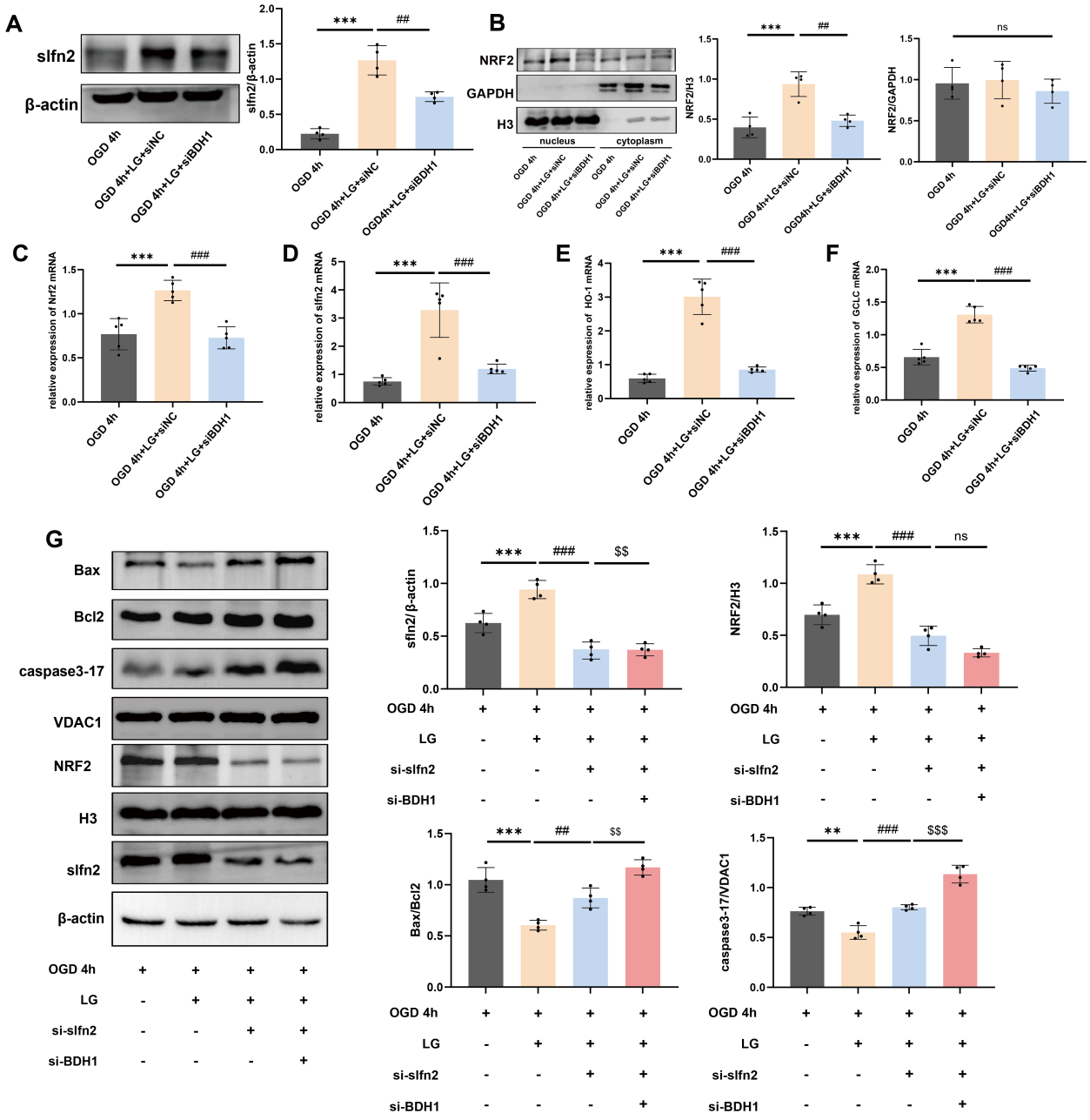



## Figure 5

Transcriptomic profiling reveals astrocytic BDH1 as a critical regulator of redox homeostasis and mitochondrial function.

(A) qPCR analysis of glucose and lipid transport-related genes (Cpt1, Cpt2, Pgc-1α, Glut3) in astrocytes . (n = 4). (B) Relative mRNA expression of ketone body-related genes (Acat1, Scot, Bdh1) in astrocytes

under LG stimulation. (n = 5). (C) BDH1 protein expression in astrocytes exposed to decreasing glucose concentrations combined with OGD, assessed by western blot. (n =5) (D) Immunofluorescence co-staining of BDH1 (red) and GFAP (green) in astrocytes under Ctrl and LG conditions, with quantification of BDH1 fluorescence intensity. Scale bar, 50 μm(n =5). (E) Principal component analysis (PCA) of transcriptomic profiles from si-NC and si-BDH1 astrocytes, showing clear separation along PC1. (F) Volcano plot of differentially expressed genes (DEGs) between si-BDH1 and si-NC groups (fold change > 1 or <−1, P < 0.05). (G) Heatmap of key DEGs, highlighting downregulation of antioxidant genes and upregulation of pro-apoptotic genes. (H) GO enrichment analysis of DEGs. (I) KEGG pathway enrichment analysis. (J) Reactive oxygen species (ROS) levels in astrocytes. (n =5) (K) Malondialdehyde (MDA) levels in astrocytes across the indicated groups. (n =4) (L) Superoxide dismutase (SOD) activity in astrocytes across the indicated groups. (n =4) (M-N) Immunofluorescence co-localization of GFAP, TOM20, and Bax with quantification.Scale bar, 20 μm (n =5) (O-P) representative fluorescence images and quantification of JC-1 aggregate/monomer ratio. Scale bar, 50μm(n =5) (Q) Transmission electron microscopy (TEM) images of neuronal mitochondria in the peri-infarct cortex of sham and I/R mice. Red arrows indicate mitochondria with vacuolation, outer membrane damage, or cristae disruption. Scale bar, 5μm. $^{\#}P<0.05$; $^{*}P<0.05$; $^{**}P<0.01$; $^{***}P<0.001$;$^{\#\#}P<0.01$; $^{\#\#\#}P<0.001$ Mean±SEM, T-test,One-way ANOWA, Two-way ANOWA.




## Figure 6

BDH1 activates the Slfn2/Nrf2 axis to mediate antioxidant stress and suppress mitochondrial apoptosis.

Representative western blot and quantification of Slfn2 protein levels in astrocytes (n =5); (B) Western blot analysis of nuclear NRF2 protein expression across the indicated groups, with Lamin B1 as the nuclear loading control. (n =4); (C-D) qPCR analysis of Slfn2 (C) and Nrf2 (D) mRNA levels in astrocytes

across the indicated groups. (n = 5); (E, F) qPCR analysis of the NRF2 downstream antioxidant genes Ho-1 (E) and Gclc (F). (n = 5); (G) Western blot analysis of nuclear NRF2, Bax, and cleaved Caspase-3 protein expression in astrocytes. (n =4). $^{\#}P<0.05$; $^{*}P<0.05$; $^{**}P<0.01$; $^{***}P<0.001$;$^{\#\#}P<0.01$; $^{\#\#\#}P<0.001$ Mean±SEM, T-test,One-way ANOWA, Two-way ANOWA.

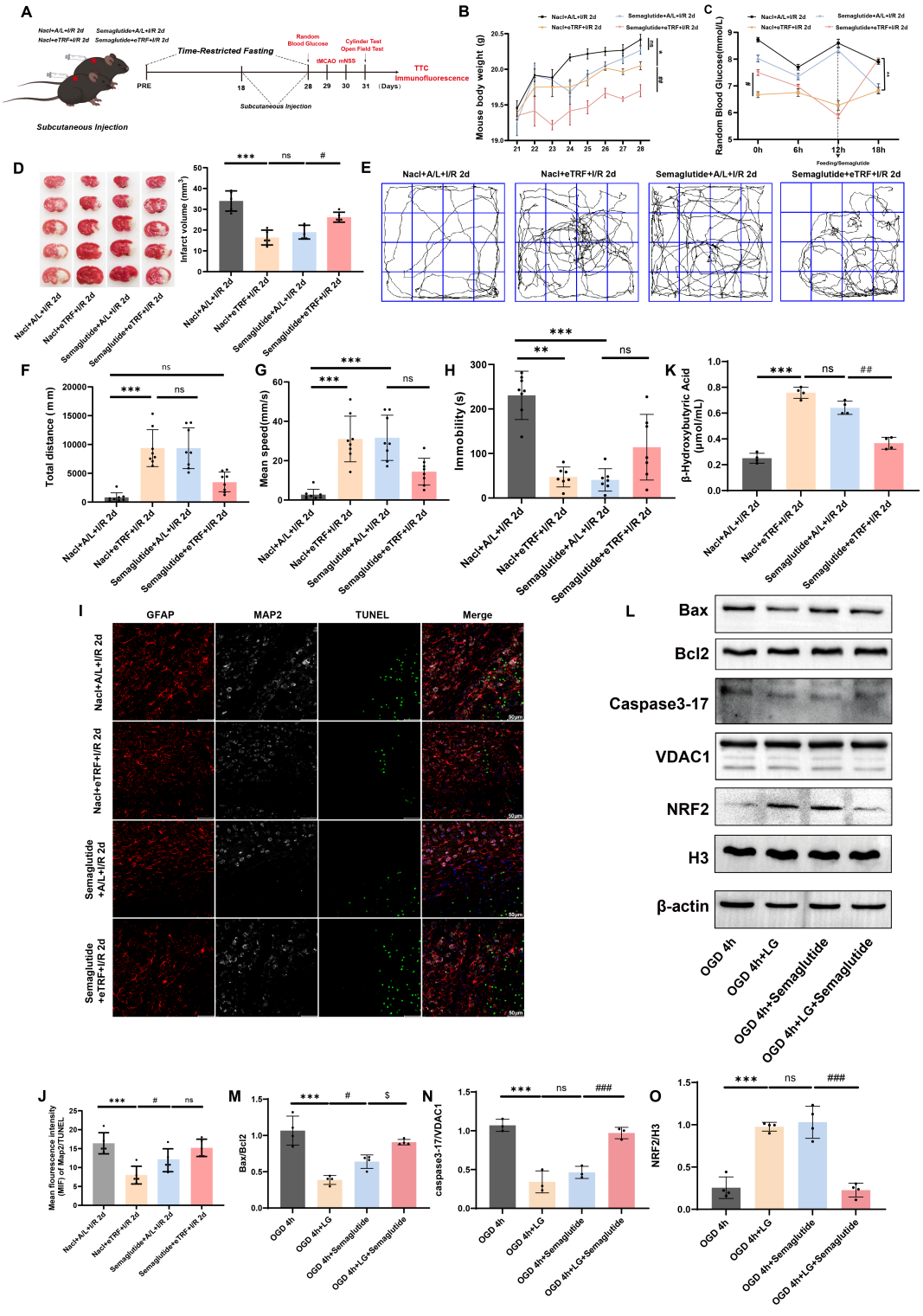



**Figure 7**

Semaglutide partially recapitulates eTRF-mediated neuroprotection against cerebral ischemia–reperfusion injury through glycemic regulation.

(A) Experimental design and treatment schedule for semaglutide administration and eTRF intervention. (B) Body weight.(n=5). (C) Random blood glucose monitoring profiles across the indicated groups.(n=5) (D) Representative TTC-stained brain sections and quantification (n =5). (E) Representative locomotor trajectories in the open field test. (F–H) Quantification of total distance traveled (F), mean speed (G), and immobility time (H) (n = 8). (I) Representative immunofluorescence images of TUNEL (green) co-stained with GFAP (red) or MAP2 (red) in the peri-infarct cortex. Scale bar, 50 μm. (J) Quantification of $TUNEL^{+}GFAP^{+}$astrocytes and $TUNEL^{+}MAP2^{+}$neurons. (n =5). (K) Serum β-hydroxybutyrate levels. (n =4). (L) Western blot analysis of cleaved Caspase-3 and Bax protein levels in astrocytes. (M-O) Western blot and quantification of BDH1, Slfn2, and nuclear NRF2 protein expression in astrocytes (n = 4). Data are presented as mean ± SEM. Statistical comparisons were performed using one-way or two-way ANOVA with appropriate post-hoc corrections. $^{\#}P<0.05$; $^{*}P<0.05$; $^{**}P<0.01$; $^{***}P<0.001$;$^{\#\#}P<0.01$; $^{\#\#\#}P<0.001$ Mean±SEM, T-test,One-way ANOWA, Two-way ANOWA.

## Supplementary Files

This is a list of supplementary files associated with this preprint. Click to download.

- Supplementarytable.docx
- SupplementaryFigure.docx
- GraphicalAbstract.png